HHS Public Access

Author manuscript

Nature. Author manuscript; available in PMC 2023 November 23.

Published in final edited form as:

Nature. 2023 April ; 616(7957): 510–519. doi:10.1038/s41586-023-05910-2.

Plastic and stimulus-specific coding of salient events in the central amygdala

Tao Yang[1,#,*], **Kai Yu**[1,*], **Xian Zhang**[1], **Xiong Xiao**[1], **Xiaoke Chen**[2], **Yu Fu**[3], **Bo Li**[1,#]

[1]Cold Spring Harbor Laboratory, Cold Spring Harbor, NY 11724, USA

[2]Department of Biology, Stanford University, California 94305, USA

[3]Institute of Molecular and Cell Biology, Agency for Science, Technology and Research (A*STAR), Singapore, 138667

Abstract

The central amygdala (CeA) is implicated in a range of mental processes including attention, motivation, memory formation and extinction, and in behaviors driven by either aversive or appetitive stimuli[1-7]. How it participates in these divergent functions remains elusive. Here we show that somatostatin-expressing (Sst^+) CeA neurons, which mediate much of CeA functions[3,6,8-10], generate experience-dependent and stimulus-specific evaluative signals essential for learning. The population responses of these neurons in mice encode the identities of a wide range of salient stimuli, with the responses of separate subpopulations selectively representing the stimuli that have contrasting valences, sensory modalities, or physical properties (e.g., shock and water reward). These signals scale with stimulus intensity, undergo pronounced amplification and transformation during learning, and are required for both reward and aversive learning. Notably, these signals contribute to dopamine neurons' responses to reward and reward prediction error, but not to their responses to aversive stimuli. Consistently, Sst^+ CeA neuron outputs to dopamine areas are required for reward learning, but are dispensable for aversive learning. Our results suggest that Sst^+ CeA neurons selectively process information about differing salient events for evaluation during learning, supporting the diverse roles of the CeA. In particular, the information for dopamine neurons facilitates reward evaluation.

Extensive studies indicate that the CeA is essential for the establishment of adaptive behaviors motivated by emotionally significant stimuli. Indeed, lesion or inhibition of the CeA impairs learning and expression of responses to approach appetitive stimuli or avoid aversive stimuli, whereas stimulation in the CeA promotes these behaviors[1-7]. Moreover, *in vivo* recording shows that CeA neurons respond to appetitive or aversive stimuli, such

[#]**Correspondence and requests for materials** should be addressed to T.Y. (tyang@cshl.edu) or B.L. (bli@cshl.edu).

[*]These authors contributed equally

Author Contributions

T.Y., K.Y. and B.L. conceived and designed the experiments. T.Y. built the wide-field microscope for *in vivo* imaging with GRIN lenses and conducted *in vivo* imaging experiments and imaging data analysis. K.Y. conducted *in vivo* optogenetic inhibition, tracing and fiber photometry experiments. X.Z. and X.X. wrote MATLAB (2017a) codes for some of the imaging analysis. X.C. developed the AAVs for retrogradely targeting CeA neurons. Y.F. developed the $Slc6a3^{Flp}$ mouse line. T.Y. and B.L. wrote the paper with inputs from all authors.

Competing interests

The authors declare no competing interests.

as water (to a thirsty animal) or shock, as well as cues predictive of these stimuli[11-20]. Such stimuli are salient, carrying affective valences (positive and negative), and also have different sensory and physical features. A fundamental question is how the CeA processes various salient stimuli and contributes to the divergent behavioral responses to these stimuli. One possibility is that CeA neurons are generally involved in common cognitive functions, such as attention or motivation[4,9,13,15,17], and therefore are important for processing diverse stimuli. Alternatively, the CeA may possess functionally distinct neuronal types or circuits, which selectively process stimuli on the basis of their affective, sensory, and physical attributes (e.g., valences, modalities, and qualities) and therefore are differentially involved in specific behavioral responses.

Sst^+ CeA neurons, defined by their expression of the neural peptide somatostatin[21], are the largest genetically identified neuronal population in the CeA, accounting for about 50% of all neurons in CeA lateral subdivision (CeL)[6,22], an amygdala nucleus required for learning[11,12,23]. These neurons send long-range projections to a number of targets and play critical roles in learning both aversive and appetitive behaviors[16-18,22,24-31], which reflect many of the divergent functions of the CeA[3,6,8,9]. However, to date the *in vivo* responses of individual Sst^+ CeA neurons to stimuli spanning affective, sensory, and physical parameter spaces have not been characterized. How these neurons and their projections take part in divergent behavioral responses is also unclear. We reasoned that addressing these issues would open a window on the precise functionality of the CeA and its circuits during behavior.

Stimulus-specific encoding in the CeA

We set out to characterize the *in vivo* activities of Sst^+ CeA neurons at cellular resolution in behaving animals. For this purpose, we delivered the genetically encoded calcium indicator GCaMP6[32] selectively into these neurons by injecting the CeA of Sst^{Cre} mice with an adeno-associated virus (AAV) expressing GCaMP6 in a Cre-dependent manner, followed by implanting a gradient-index (GRIN) lens into the same location (Extended Data Fig. 1a-d). Four to six weeks later, we imaged the GCaMP6 signals (which represent neuronal activities) in the infected neurons through the GRIN lens (Methods). During imaging, we presented the mice with batteries of stimuli that differed in valences, sensory modalities, or physical properties (first battery: water, sucrose solution, food pellets, and tail shock (Fig. 1a-c; Extended Data Fig. 1e); second battery: water, sucrose solution, quinine solution, air puff, and tail shock (Extended Data Fig. 1f-h; Methods)).

Notably, many neurons were highly selective, showing excitatory responses to the delivery of only one of these stimuli (Extended Data Fig. 1e). Hierarchical clustering based on neuronal activities grouped the neurons that preferentially responded to a specific stimulus, such as water, sucrose, food, shock, or quinine (Fig. 1a-c; Extended Data Fig. 1f-h), although some neurons responded to multiple stimuli. Correlation analysis revealed that individual neurons showed largely uncorrelated responses to stimuli that have different valences and sensory or physical properties (e.g., sucrose vs. shock, or water vs. food), and subsets of neurons showed correlated responses to stimuli with similar attributes (e.g., water and sucrose solution; Extended Data Fig. 1i, j). However, even for stimuli

with similar attributes (e.g., regular and sweet food pellets, Fig. 1d-f), population analysis with dimensionality reduction (Methods) showed that the trajectories of the trial-by-trial responses were clearly separable according to individual stimuli (Fig. 1g). Furthermore, the population responses could be used to decode the stimuli on a trial-by-trial basis (Fig. 1h; Methods). These results demonstrate that Sst^+ CeA neuron population activities contain sufficient information to code the identities of a wide range of stimuli.

The representation of contrasting stimuli

The clustering and correlation analyses depict overall response profiles, and suggest that individual Sst^+ CeA neurons may have mixed selectivity depending on the similarity between stimuli (Fig. 1a-c; Extended Data Fig. 1f-j). We next more precisely assessed the selectivity of individual Sst^+ CeA neurons to water and shock, which are often used as unconditioned stimuli (USs) in learning tasks, and which have opposing valences and different sensory/physical properties. We found that many neurons were selectively excited by either water or shock, whereas only a small fraction was excited by both stimuli defined based on trial-by-trial statistics (Fig. 1i, left; Methods). Almost no neurons showed inhibitory responses (Fig. 1i, right). Interestingly, the neurons excited by different stimuli displayed differential patterns of spatial distribution in the CeA, with the shock-excited neurons being more dispersed than water-excited neurons (Extended Data Fig. 1k, l; Methods).

The responses of the water-excited neurons and shock-excited neurons scaled with water volume and shock intensity, respectively (Fig. 1j-m), indicating that the two groups of neurons separately represent the strength of the two stimuli. While many neurons were responsive to either water or shock, very few were responsive to an insignificant neutral stimulus (e.g., sound; Extended Data Fig. 1m). Notably, the activities of almost all water-excited neurons arose later than animal's licking responses following water delivery, with lags of at least 300 ms (Extended Data Fig. 1n-p; Methods). Moreover, the activities of most neurons did not correlate with licking rate following water delivery (Extended Data Fig. 1q, r). These results and those described later (Extended Data Fig. 1s-ff) suggest that Sst^+ CeA neuron endogenous activities do not drive or represent the vigor of licking. Together, these results indicate that separate subsets of Sst^+ CeA neurons represent the strength of contrasting salient stimuli (such as water and shock) in a stimulus-specific manner.

Learning amplifies responsiveness to USs

To understand how Sst^+ CeA neurons participate in behaviors driven by divergent salient stimuli, we imaged their activities during Pavlovian conditioning (Fig. 2a; Methods). We trained mice first in reward conditioning, in which a conditioned stimulus (CS_{WA}, a sound) predicted the delivery of an unconditioned stimulus (US_{WA}, water). After several sessions of training, the same mice were subjected to fear conditioning, in which CS_{SH} (a different sound) predicted the delivery of a tail shock (US_{SH}). After (but not before) the training, mice showed licking and pupil enlargement in response to CS_{WA} and CS_{SH}, respectively, indicating the formation of both appetitive and aversive associations (Extended Data Fig. 2a, b).

Very few neurons showed any inhibitory responses to the CSs or USs throughout the training (Extended Data Fig. 2c). After the training, some Sst^+ CeA neurons showed excitatory response to CS_{WA} or CS_{SH}, with the majority also excited by US_{WA} or US_{SH}, respectively (Fig. 2b, c; Extended Data Fig. 2d). The CS_{WA}- or CS_{SH}-excited populations were largely nonoverlapping, as were the US_{WA}- or US_{SH}-excited populations (Fig. 2c). Interestingly, training not only increased the number of CS_{WA}- or CS_{SH}-excited neurons, but also increased the number of US_{WA}-excited neurons (Fig. 2d). Next, we inspected the neurons that were trackable during the reward or fear conditioning (Extended Data Fig. 2e-j; Methods). Among the tracked neurons – which constituted a substantial fraction of responsive neurons (Extended Data Fig. 2g) – all those excited by CS_{WA} after training were initially not responsive to CS_{WA}, and half of those excited by US_{WA} after training were also initially not responsive to US_{WA} (Extended Data Fig. 2h), consistent with a training-induced potentiation of US-responsiveness.

CS-US associative learning appears to be crucial for the potentiation of US-responsiveness, as simple repeated exposures to positive or negative USs failed to increase the number of US-responsive neurons, or change the compositions of neurons responsive to different USs (Extended Data Fig. 2k-m). Interestingly, although individual neurons may change their preferred stimuli across days, a water-excited neuron almost never became a shock-excited neuron, and vice versa (Extended Data Fig. 2n-p). These results together indicate that learning not only gives rise to CS-responsive neurons, but also amplifies the pool of US-responsive neurons.

Learning transforms CeA neuron responses

To examine the effect of training on population responses, we performed dimensionality reduction on the activities of all the tracked neurons and represented the CS_{WA}- or US_{WA}-evoked responses in the activity space, both before and after training (Extended Data Fig. 2i). We computed the Mahalanobis distance (MD) between the response vectors as a measure of similarity (Methods). Training decreased the MD (Extended Data Fig. 2j), suggesting that learning increases the similarity between CS responses and the responses to the entraining US.

Consistently, analysis on all the recorded neurons revealed that CS-excited neurons significantly overlapped with US-excited neurons after learning (CS_{WA}/US_{WA}, P = 0.004; CS_{SH}/US_{SH}, P = 1.2e-06, Fisher's exact test; Fig. 2c). The trial-by-trial trajectories of Sst^+ CeA neuron population responses to US_{WA} were markedly different from those to US_{SH}, and the responses can be used to decode water and shock (Fig. 2e-g). Similarly, the trajectories of the population responses to CS_{WA} were separated from those to CS_{SH} after learning, and the CS responses can also be used to decode the upcoming water and shock, with decoding accuracy dependent on learning (Fig. 2h-l).

Could the separation between CS_{WA} and CS_{SH} responses be caused by the fact that US_{WA} and US_{SH} are drastically different in valences and sensory modalities? To address this question, we exploited two positive USs in the same modality for training. We trained new mice in a two-alternative choice (2AC) task where CS_{WA} predicted water (US_{WA}) delivery

from one spout, and CS_{SU} predicted sucrose solution (US_{SU}) delivery from another spout (Fig. 2m-o; Methods). Sst^+ CeA neuron responses in this task (Fig. 2p-z) resembled those in Pavlovian conditioning. In particular, the population responses to US_{WA} were markedly different from those to US_{SU}, and the responses can be used to decode water and sucrose solution (Fig. 2s-u). Similarly, the population responses to CS_{WA} were separated from those to CS_{SU} after learning, and the CS responses can also be used to decode the upcoming water and sucrose in a learning-dependent manner (Fig. 2v-z). These results suggest that learning transforms Sst^+ CeA neuron CS responses such that they match or predict US responses, and also confirm that learning increases the number of US-responsive Sst^+ CeA neurons (Fig. 2q, r).

Stimulus-specific extinction signals

To further examine the relationship between neuronal response and behavior, we tested mice for memory retrieval after Pavlovian conditioning wherein the CSs were presented without the delivery of USs (i.e., in extinction). Mice displayed licking and blinking responses to CS_{WA} and CS_{SH}, respectively, especially in the early trials, indicating that the appetitive and aversive memories were maintained (Extended Data Fig. 3a, b). We detected two largely nonoverlapping populations, with one excited by CS_{WA} but not CS_{SH}, and the other by CS_{SH} but not CS_{WA} (Extended Data Fig. 3c-e). The population activities evoked by the CSs can be used to accurately classify trial types (Extended Data Fig. 3f). These results are largely consistent with the findings from the conditioning phase (Fig. 2a-l).

During reward memory retrieval, animal's licking response was high in early trials and low in late trials (Extended Data Fig. 3g, h), reflecting extinction. Remarkably, two types of neurons emerged, with one being excited by CS_{WA} in early trials but becoming silent in late trials, and the other being silent in early trials but becoming excited by CS_{WA} in late trials (when licking responses were extinguished) (Extended Data Fig. 3i-k). Similarly, during aversive memory retrieval, animal's blinking response was high in early trials and low in late trials (Extended Data Fig. 3l, m). There were also two types of neurons: one that was excited by CS_{SH} in early trials but became silent in late trials, and the other that was silent in early trials but became excited by CS_{SH} in late trials (when blinking responses were extinguished) (Extended Data Fig. 3n-p). Interestingly, during either conditioning or retrieval (Extended Data Fig. 1s-bb), the CS responses in all the neurons occurred later than the behavioral responses (licking or blinking) induced by the same CS, and the responses of most of these neurons did not correlate with the behavioral responses. These results support the notion that the activities of these neurons unlikely initiate or invigorate actions. The neurons specifically excited by CS in the late trials of retrieval resemble the previously described "extinction neurons" in the CeA[12,13]. However, our results extend previous findings and indicate that CeA extinction neurons are highly specific, with different subpopulations separately representing the extinction of distinct USs.

Learning-dependent evaluative signals

To further understand how CeA neuron response evolves and participates in instrumental learning, we trained additional mice in a "go/no-go" task (Extended Data Fig. 4a; Methods).

In the go trials, a sound (CS_{SU}) indicated that sucrose (US_{SU}) would be delivered. In the no-go trials, another sound (CS_{QU}) announced that quinine (US_{QU}) would be delivered. With training, mice were able to acquire appropriate actions, licking following CS presentation in almost all go trials to obtain sucrose, and withholding licking in the majority of no-go trials to avoid quinine (Fig. 3a). Thus, training effectively increased "hit" and "correct rejection (CR)", and correspondingly reduced "miss" and "false alarm (FA)" across animals (Extended Data Fig. 4b).

We imaged the activities of Sst^+ CeA neurons at different stages of training (Fig. 3b-j; Extended Data Fig. 4c, d). While US-excited neurons greatly outnumbered CS-excited neurons at all stages, training increased both populations (Fig. 3b, c; Extended Data Fig. 4c, d). The neurons excited by different USs were largely nonoverlapping, as were those excited by different CSs (Fig. 3c). Notably, almost no neuron was excited by CS_{QU} in CR trials, even at the late stage when the same CS did excite neurons in FA trials (Fig. 3b; Extended Data Fig. 4d). In both hit trials and FA trials, the CS responses in most neurons occurred later than licking responses, and did not correlate with licking (Extended Data Fig. 1cc-ff). Very few neurons were inhibited by any of the stimuli (Extended Data Fig. 4e).

To verify the effects of training, we tracked individual neurons across stages. Many neurons were initially not responsive to any of the CSs, but became excited by the same CSs after training (Fig. 3d; Extended Data Fig. 4f). Similarly, many US-nonresponsive neurons became US-excited. As a result, new and enlarged populations of US-excited neurons emerged at the late stage (Fig. 3e). Consistent with the above observation, the CS-excited neurons in FA trials were not responsive in CR trials (Fig. 3d, right; Extended Data Fig. 4f). One interpretation is that these neurons only fire when a salient event is expected to occur, but remain silent if nothing is expected.

To visualize how the responses of Sst^+ CeA neurons in hit, CR and FA trials develop during learning, we projected the population activities of Sst^+ CeA neurons along a coding direction, which optimally separated the activities during anticipation of outcomes in different trial types (Methods). Robust and sustained predictive signals in hit trials can be well separated from the signals in CR or FA trials in a training-dependent manner (Fig. 3f). Correspondingly, the trajectories of Sst^+ CeA neurons in activity space during the CS period in hit, CR and FA trials were markedly different from each other in the late stage of training (Fig. 3g, h). Remarkably, training also further separated the population activities during the US period between hit trials and CR trials, and between hit trials and FA trials (Fig. 3i, j).

These results confirm that the responses of different Sst^+ CeA subpopulations represent contrasting USs (and the associated CSs) in a learning-dependent and stimulus-specific manner, and that such responses unlikely drive or invigorate actions. Interestingly, although these neurons are silent if no US is expected (e.g., in CR trials), many fire when an expected US is omitted (e.g., during extinction; Extended Data Fig. 3). Taken together, we reasoned that Sst^+ CeA neurons participate in evaluating the USs during learning.

The US responses facilitate learning

To test this hypothesis, we sought to optogenetically inhibit Sst^+ CeA neurons specifically in the US presentation window during learning. We infected these neurons bilaterally with an AAV expressing the light-sensitive proton pump archaerhodopsin (ArchT), or GFP (as the control), and implanted optical fibers above the infected areas for light delivery (Fig. 4a). The mice were first trained in reward conditioning, and subsequently in the go/no-go task (Fig. 4b). During training, a pulse of green light was delivered into the CeA immediately following US presentation (Methods).

Strikingly, the ArchT group had lower performance and less anticipatory licking than the GFP group during reward conditioning training (Fig. 4c, d), indicating that inhibiting Sst^+ CeA neurons during reward consumption impairs learning. These mice were then given additional training in the absence of light stimulation, allowing them to reach similar levels of performance and anticipatory licking responses (Fig. 4e). Both groups were then trained in the go/no-go task in the presence of the light stimulation. Across training sessions, the ArchT group had reduced hit rate and anticipatory licking in response to the go-cue (CS_{SU}), and increased FA rate and licking induced by the no-go cue (CS_{QU}) (Fig. 4f, g). These results indicate that both reward learning and aversive learning are impaired by inhibiting Sst^+ CeA neurons during US consumption.

To test whether US responses of Sst^+ CeA neurons are required for expressing learned behavior, we continued to train these mice without light stimulation until the two groups reached similar levels of performance and licking responses in the go and no-go trials (Extended Data Fig. 5a, b). We then tested these mice with the light stimulation. The ArchT mice and GFP mice had similar performance and licking responses in both the go and no-go trials (Extended Data Fig. 5c-g), indicating that inhibiting Sst^+ CeA neurons during US presentation does not affect well-learned behavior.

We next tested whether the CS responses are required for expressing learned behavior. A new batch of mice were prepared and trained in the reward conditioning and go/no-go task (Methods). In either task, animals' performance and anticipatory licking responses were not affected by Sst^+ CeA neuron inhibition during CS presentation (Extended Data Fig. 5h-o). These results suggest that the CS responses of Sst^+ CeA neurons are not required for executing well-learned behavioral responses.

In additional control experiments, we found that inhibiting Sst^+ CeA neurons did not induce aversive (or preference) responses, or affect animals' licking behavior (Extended Data Fig. 5p-t), suggesting that this manipulation by itself is not aversive and does not affect motor functions. Together, these results indicate that Sst^+ CeA neurons are essential for both reward and aversive learning, but are less important for the expression or execution of specific behavioral actions once the actions have been established.

$Sst^{CeA \rightarrow DA}$ is needed for reward learning

CeA neurons send projections to midbrain dopamine (DA) areas, including the substantia nigra pars compacta (SNc) and the ventral tegmental area (VTA)[16,17,33-38]. A recent study

shows that these projections are required for both reward learning and fear conditioning[17]. Therefore, we examined whether some of the functions of Sst^+ CeA neurons are mediated by this pathway. We first verified that these neurons indeed send projections to DA areas (Extended Data Fig. 6a-h). Notably, CeA projections to the SNc originate mainly from Sst^+ neurons (Extended Data Fig. 6c-e), whereas those to the VTA originate from both Sst^+ neurons and Sst-negative (Sst^-) neurons, with the majority of Sst^- neurons located within CeA medial subdivision (CeM) (Extended Data Fig. 6f-h).

To determine whether the Sst^+ CeA neurons projecting to DA areas ($Sst^{CeA\rightarrow DA}$) can convey US information, we selectively labeled these neurons with GCaMP6 using an intersectional viral approach (Extended Data Fig. 7a-d; Methods). Like the general Sst^+ CeA population, subsets of $Sst^{CeA\rightarrow DA}$ neurons were excited by water or sucrose with mixed selectivity and correlative responses, while another subset showed selective responses to shock (Extended Data Fig. 7e-i). In particular, the neurons excited by shock and those excited by water or sucrose were completely nonoverlapping (Extended Data Fig. 7j, k). These results suggest that $Sst^{CeA\rightarrow DA}$ neurons transmit information about the positive and negative USs to DA areas through separate channels.

We then assessed whether $Sst^{CeA\rightarrow DA}$ projections are required for learning. We expressed ArchT in Sst^+ CeA neurons and implanted optical fibers bilaterally above the SNc for optogenetic inhibition (Fig. 5a). Inhibition of $Sst^{CeA\rightarrow DA}$ specifically during US presentation impaired learning in the reward task (Fig. 5b). However, once the reward task had been learned, the same manipulation failed to have an effect on learning in the go/no-go task (Extended Data Fig. 5u-w). We further trained these mice in a classical fear conditioning paradigm, in which we inhibited $Sst^{CeA\rightarrow DA}$ during shock presentation (Fig. 5c). This manipulation did not affect fear memory formation, albeit it slightly enhanced freezing during conditioning. These results suggest that $Sst^{CeA\rightarrow DA}$ projections are required for reward learning, but are dispensable for aversive learning.

The sufficiency to promote DA activity

To determine whether $Sst^{CeA\rightarrow DA}$ projections act by regulating DA neurons, which instruct reward learning[39,40], we first conducted anterograde transsynaptic tracing of Sst^+ CeA neurons with a monosynaptic herpes simplex virus (HSV) (Extended Data Fig. 6i-l; Methods). We found that Sst^+ CeA neurons make monosynaptic connections predominately with putative GABAergic neurons in the SNc and VTA, but rarely with DA neurons, suggesting that Sst^+ CeA neurons may inhibit GABAergic neurons in these midbrain areas, thereby disinhibiting DA neurons.

We tested this possibility by activating Sst^+ CeA neurons while simultaneously recording DA neuron activity. We used $Sst^{Flp};Slc6a3^{Cre}$ or $Sst^{Cre};Slc6a3^{Flp}$ mice, which enabled selective expression of ChR2 (the light-gated cation channel channelrhodopsin) and GCaMP6 in Sst^+ CeA neurons and DA neurons, respectively, in the same animals (Fig. 5d; Extended Data Fig. 8a; Methods). Optical fibers were implanted above the CeA and the DA areas for photo-stimulation and photometry, respectively (Extended Data Fig. 8l-o). Remarkably, brief light pulses delivered to the CeA reliably triggered excitatory responses

in dopamine neurons in both the VTA (Fig. 5d-g; Extended Data Fig. 8j, k) and the SNc (Extended Data Fig. 8a-d, h, i), without inducing any licking responses. In contrast, providing the same mice with water triggered both dopamine neuron excitation and licking (Fig. 5h-j; Extended Data Fig. 8e-g). These results show that Sst^+ CeA neurons are sufficient to promote DA neuron activity, likely through inhibiting GABAergic neurons in the VTA and SNc.

The necessity for endogenous DA activity

Are Sst^+ CeA neurons also required for DA neuron activity? We addressed this question by chemogenetically inhibiting Sst^+ CeA neurons while imaging dopamine neuron activity in the $Sst^{Cre};Slc6a3^{Flp}$ mice, which allow selective expression of KORD (an inhibitory DREADD derived from the kappa-opioid receptor)[41] and GCaMP6 in Sst^+ CeA neurons and dopamine neurons, respectively, in the same animals (Fig. 5k-u; Extended Data Fig. 9 & 10). A GRIN lens was implanted into the VTA for the imaging.

We tested the effects of Sst^+ CeA neuron inhibition by systemic application of salvinorin B (SALB), the agonist of KORD[41]. Remarkably, this manipulation markedly reduced DA neuron responses to water and sucrose, but did not affect their responses to shock or quinine (Fig. 5l-o; Extended Data Fig. 9). We then trained the mice in the reward conditioning task, after which we presented the mice with expected or unexpected reward while imaging DA neuron activities with or without the inhibition of Sst^+ CeA neurons (Extended Data Fig. 10a-d). The inhibition markedly reduced DA neuron responses to the CS and the expected reward (Fig. 5p-u). Interestingly, the inhibition also reduced the responses of DA neurons – including all the identified prediction error (PE)-encoding neurons (Fig. 5p-s; Extended Data Fig. 10e, f) – to the unexpected reward (Fig. 5p-u). Control experiments confirmed that vehicle treatment did not affect DA neuron responses and animal behavior (Fig. 5k-u; Extended Data Fig. 9 & 10). These results indicate that the endogenous Sst^+ CeA neuron activities are required for DA neuron response to reward or reward PE; however, they are not required for DA neuron response to aversive stimuli.

Discussion

Our results uncover previously unappreciated coding capacity of CeA neurons, showing that population activities of Sst^+ CeA neurons encode the identities of a wide range of salient stimuli. Individual Sst^+ CeA neurons may have mixed selectivity, especially for stimuli that have both the same valence and similar sensory/physical properties. Nevertheless, a substantial number of these neurons are capable of discriminating between stimuli that clearly differ in either affective or sensory/physical properties. Thus, separate subsets of Sst^+ CeA neurons are selectively excited by either water or shock (or by either sucrose or quinine). Importantly, the number of US-excited neurons is markedly increased during learning. This amplification of US response could, in turn, be essential for learning. Consistent with this notion, inhibiting Sst^+ CeA neurons specifically during US presentations prevents both reward and aversive learning.

Our results also reveal a unique role of $Sst^{CeA\rightarrow DA}$ neurons in reward learning, which is likely mediated by their specific regulation of DA neurons. Indeed, we show that inhibition of Sst^{+} CeA neuron endogenous activities impairs DA neuron responses to reward and reward prediction error, but does not affect DA neuron responses to aversive stimuli. Consistently, Sst^{+} CeA neuron projections to dopamine areas are required for reward learning, but are not required for aversive learning.

Sst^{+} CeA neurons have other notable features. First, their responses scale with US intensity. Second, their responses lag behind animal's behavioral actions and do not correlate with action vigor. These neurons therefore markedly differ from the neurons in two major CeA input areas – the insular cortex and basolateral amygdala – whose responses precede behavioral actions[42-45] and correlate with action vigor[42]. Third, separate subsets of these neurons respond to the extinction of USs in a stimulus-specific manner. In light of all the results, we propose that a major function of Sst^{+} CeA neurons is to participate in the evaluation of various salient events during learning (or extinction). Through learning, the stimulus-specific evaluative signals from these neurons are amplified and conveyed to downstream areas, where they regulate other key players in evaluation, such as DA neurons in the midbrain[39,40].

Our results help explain the diverse roles of the CeA[3,6], especially its role in reward learning[16-18,22,24-30], and also provide *in vivo* evidence for the long-standing hypothesis that the CeA regulates midbrain DA neurons[17,46,47]. While the $Sst^{CeA\rightarrow DA}$ neurons facilitate reward learning, the precise functions of other CeA neurons remain to be elucidated. Sst^{+} CeA neurons can be further parcelled out into subclasses according to their differential gene expression profiles and spatial locations. For example, a recent study reported that the $Sst^{+}/Pdyn^{+}/Vipr2^{-}$ neurons in the lateral and capsular subdivisions of the CeA were one of the major CeA populations that project to the SNc[48]. These neurons may correspond to the $Sst^{CeA\rightarrow DA}$ neurons. Besides these neurons, a group of Sst^{-} neurons in the CeM also project to the SNc[48]. These neurons may be involved in aversive learning[16,17]. In addition, other pathways originating from Sst^{+} CeA neurons[24,28,49] may be critical for aversive learning. Future studies will need to disentangle how different CeA populations or pathways coordinate to participate in learning.

Methods

Mice

Male and female mice (2-4 months old) were used for all the experiments. Mice were housed under a 12-h light/dark cycle (7 a.m. to 7 p.m. light) with constant room temperature of 21°C and 65% humidity. Mice were housed in groups of 2-5, with the exception that those with GRIN lens implantation were housed individually. Food and water were available *ad libitum* before the start of experiments. All experiments were performed during the light cycle. Littermates were randomly assigned to different groups prior to experiments. All mice were bred onto a C57BL/6J background. All experimental procedures were approved by the Institutional Animal Care and Use Committee of Cold Spring Harbor Laboratory and performed in accordance to the US National Institutes of Health guidelines.

The *Sst*^{Cre} (stock number: 013044, strain code: *Sst*$^{tm2.1(cre)Zjh/J}$), *Sst*^{Flp} (stock number: 031629, strain code: *B6J.Cg-Sst*$^{tm3.1(flpo)Zjh/AreckJ}$), and *Slc6a3*^{Cre} (also known as DAT-Cre; stock number: 006660, strain code: *B6;SJL-Slc6a3*$^{tm1.1(cre)Bkmn/J}$) mice were purchased from The Jackson Laboratory (Bar Harbor, ME 04609, USA). The *R26*$^{LSL-H2B-GFP}$ reporter mouse line was generated by Dr. Z. Josh Huang[50].

The *Slc6a3*^{Flp} mouse line was generated by Dr. Fu Yu and is available at The Jackson Laboratory (also known as DAT-IRES-Flpo; stock number: 033673, strain code: *B6N(Cg)-Slc6a3*$^{tm1.1(flpo)Fuyu/J}$; RRID: IMSR_JAX:033673). The DAT-IRES-Flpo targeting construct was designed to insert a *loxN*-flanked neomycin resistance (neo) cassette followed by an internal ribosomal entry site (IRES) and a FlpO recombinase sequence downstream of the stop codon of the solute carrier family 6 (neurotransmitter transporter, dopamine), member 3 (*Slc6a3*) gene. This construct was electroporated into C57BL/6NCrl embryonic stem (ES) cells. Correctly targeted ES cells were injected into blastocysts and the resulting chimeric males were bred to CMV-cre mice to remove the neo cassette. Offspring were crossed with C57BL/6NCrl mice to remove the *cre*-expressing transgene, and resulting DAT-ires-Flpo mice were bred to C57BL/6NCrl mice for at least five generations.

Viruses

The pAAV-Syn-FLEX-GCaMP6f-WPRE-SV40 (AAV1, 1.0x10^13 GC/ml), pAAV-hSyn-dF-HA-KORD-IRES-mCitrine (AAV8, 2.0x10^13 GC/ml), pAAV-EF1a-DIO-hChR2-EYFP (AAV5, 2.5x10^13 GC/ml), and pAAV-hSyn-DIO-EGFP (AAV5, 1.6x10^13 GC/ml) were purchased from Addgene (Watertown, MA 02472, USA). The following AAVs were purchased from the University of North Carolina Vector Core (Chapel Hill, NC 27599, USA): rAAV9/CAG-FLEX-ArchT-GFP (4.7x10^12 GC/ml), AAV9-DIO-mRudy-GCaMP6f (7.8x10^12 GC/ml), and AAVdj-hSyn-C_{OFF}/F_{ON}-hChR2 (4.0x10^12 GC/ml). The AAV8-Ef1a-fDIO-GCaMP6m (1.59x10^13 GC/ml) was produced by K. Deisseroth's lab at Stanford University. The AAV8-retro-hsyn-mTagBFP-P2A-Cre (5.0x10^13 GC/ml) and AAV8-retro-hsyn-FLEX-mTagBFP-P2A-Flp (2.8x10^14 GC/ml) were generated by Dr. Xiaoke Chen. The rAAV-Ef1a-DIO-EGFP-2A-TK (2.66x10^12 GC/ml) and HSV-ΔTK-tdTomato (1.0x10^9 PFU/ml) were purchased from BrainVTA (Wuhan, 430000, China). All viruses were stored in aliquots at −80 °C until use. We typically waited at least 4 weeks after virus injection to allow viral expression. For the anterograde transsynaptic tracing, we first injected the rAAV-Ef1a-DIO-EGFP-2A-TK, and 20 days later injected the HSV-ΔTK-tdTomato. We waited another 5 days for the expression of tdTomato[51,52].

Stereotaxic surgery

All surgery was performed under aseptic conditions and body temperature was maintained with a heating pad. Standard surgical procedures were used for stereotaxic injection and implantation, as previously described[16,19,22,25]. In brief, mice were anaesthetized with isoflurane (2% at the beginning for induction and 1%-1.5% for the rest of the surgery), and positioned in a stereotaxic frame. The frame was linked to a digital mouse brain atlas to guide the targeting of different brain structures (Angle Two Stereotaxic System; Leica Biosystems Division of Leica, Buffalo Grove, IL 60089, USA). The following stereotaxic coordinates were used for the CeA: −1.2 to −1.3 mm from bregma, 2.9 to 3.0 mm lateral

from the midline, and 4.5 to 4.6 mm vertical from skull surface; for the SNc: −3.1 mm from bregma, 1.6 mm lateral from the midline, and 4.1 mm vertical from skull surface; and for the VTA: −3.2 mm from bregma, 0.8 mm lateral from the midline, and 4.2 mm vertical from skull surface.

For injection of virus or CTB, we made a small cranial window (1-2 mm^2), through which virus (~0.3 μl) or CTB (~0.1 μl) were delivered via a glass micropipette (tip diameter, ~5 μm) by pressure application (5-20 psi, 5-20 ms pulses at 0.8 Hz) controlled by a Picospritzer III (Parker Hannifin, Hollis, NH 03049, USA) and a pulse generator (Agilent).

For *in vivo* optogenetics, optical fiber implantation was performed after the viral injection in the same surgery. Optical fibers (core diameter, 200 μm; length, 5 mm; NA, 0.22; Inper Corporation, Hangzhou, China) were bilaterally implanted and placed 200 μm above the CeA or SNc. For *in vivo* fiber photometry, optical fiber implantation was also performed after the viral injection in the same surgery. Optical fibers (core diameter, 200 μm; length, 5 mm; NA, 0.37; Inper Corporation, Hangzhou, China) were placed unilaterally in the SNc or VTA, ipsilateral to the targeted CeA.

For *in vivo* imaging with gradient-index (GRIN) lenses, one week after viral injection, a second surgery was performed for GRIN lens implantation into the virus infected area. To implant the GRIN lens (diameter, 600 μm; length: 7.3 mm; Inscopix, Palo Alto, CA 94303, USA), we first enlarged the cranial window using a thrill, and then used a holder (Inscopix) to hold and carefully lower the GRIN lens through the window into the target area at a low speed (~100 μm/min). We subsequently fixed the GRIN lens in place using metabond (Parkell Products Inc, Edgewood, NY, USA) and dental cement (Lang Dental Manufacturing Company, Wheeling, Illinois, USA). The holder was released until the cement was completely cured. A metal head-bar (for head-restraint in all the mice used in the imaging and behavioral experiments) was subsequently mounted onto the skull with black dental cement. We waited for a minimum of 6 weeks before starting the imaging experiments in these mice.

Immunohistochemistry

Immunohistochemistry experiments were conducted following standard procedures[53]. Briefly, mice were anesthetized with Euthasol (0.4 ml; Virbac, Fort Worth, Texas, USA) and transcardially perfused with 30 ml of PBS, followed by 30 ml of 4% paraformaldehyde (PFA) in PBS. Brains were extracted and further fixed in 4% PFA overnight followed by cryoprotection in a 30% PBS-buffered sucrose solution for 48 h at 4 °C. Coronal sections (40 or 50 μm) were cut using a freezing microtome (Leica SM 2010R, Leica).

Sections were first washed in PBS (5 min), incubated in PBST (0.3% Triton X-100 in PBS) for 30 min at room temperature (RT) and then washed with PBS (3 x 5 min). Next, sections were blocked in 2% normal goat serum in PBST for 30 min at RT and then incubated with primary antibodies overnight at 4 °C. Sections were washed with PBS (3 x 5 min) and incubated with fluorescent secondary antibodies at RT for 2 h. After washing with PBS (3 x 5 min), sections were mounted onto slides with Fluoromount-G (eBioscience, San Diego, California, USA). Images were taken using a LSM 710 laser-scanning

confocal microscope (Carl Zeiss, Oberkochen, Germany). The primary antibodies used were: chicken anti-GFP (Aves Labs, catalogue number GFP1020, lot number GFP697986; dilution 1:1000), rabbit anti-Somatostatin-14 (T-4103, Peninsula Laboratories; dilution 1:1000), anti-HA-Tag (C29F4) rabbit mAb (Cell Signaling, catalogue number 3724; dilution 1:1000), anti-tyrosine hydroxylase (EMD Millipore, catalogue number AB152, lot number 3075678; dilution 1:1000), anti-BFP (AB233, Evrogen, lot number 23301171269; dilution 1:1000). Fluorophore-conjugated secondary antibodies used were: AF488-conjugated goat anti-chicken (Thermo Fisher, catalog number A-11039; dilution 1:1000); AF594-conjugated goat anti-rabbit (Thermo Fisher, catalog number A-11012; dilution 1:1000).

Behavioral tasks

Feeding mice with food pellets—To image the responses of neurons to food consumption, a custom-built pellet dispenser was used to deliver food pellets to mice. An external trigger signal from a Bpod State Machine (Sanworks, Rochester, NY 14604, USA) was used to synchronize pellet delivery with the imaging. Each time the pellet dispenser receives a trigger, a pellet would be delivered to mice through a long tube connected to the dispenser.

A food-restriction schedule started 23 h before training. Mice were first habituated in a head-restraint frame for 10 min each day for two days. On day 3, mice were trained to eat the pellets made of regular chow (i.e., the regular pellets) that were delivered in front of the mouth by the pellet dispenser. Once mice have learned to successfully obtain the pellets in at least 85% of the trials, we started to deliver two types of pellets to the mice, the regular pellets and sweet pellets, which had similar physical properties except the tastes (20 mg per pellet; Bio-serv, NJ 08822, USA). In each trial only one pellet was delivered, with the type of the pellet being randomly chosen.

Pavlovian conditioning task—A water-restriction schedule started 23 h before training in the auditory Pavlovian conditioning task under head-restraint. Mice were first habituated in a head-restraint frame for 10 min each day for two days. On day 3, mice were trained to lick for water from a metal spout placed in front of the mouth. Once mice have learned to successfully obtain water from the spout, they were habituated to an auditory conditioned stimulus (CS_{WA}; 1 s, 4 kHz, 70dB) for 20 trials in one session. 24 hours later, mice were subjected to reward conditioning. In each trial, the 1-s CS_{WA} was presented, followed by a delay and then a water reward (US_{WA}; 5 μl). The delay started with 0.5 s and increased daily until it reached 1.5 s. Mice were conditioned for at least 80 trials per day, with variable inter-trial-intervals (1-3 s). Mice were considered to have fully learned the task once they reached 85% performance (i.e., licked the spout during the delay between CS_{WA} and US_{WA} at least once every trial in all trials). The reward conditioning was continued for three more days after mice have fully learned the task.

In each of these three days, the mice were provided with free water immediately following the last trial of the reward conditioning till they were sated, and then subjected to auditory fear conditioning. Specifically, on the first day of these three days, once mice were sated, they were habituated to another auditory conditioned stimulus (CS_{SH}; 1 s, 10 kHz, 70 dB)

for 20 trials. Mice were subsequently subjected to 15 trials of fear conditioning. In each trial of the conditioning, the 1-s CS_{SH} was presented, followed by a 1.5-s delay and then a tail shock (US_{SH}; 0.5 mA for 500 ms). The inter-trial-intervals were variable (1-3 s). In the remaining two days, mice were subjected to the same procedure, except that the habituation was omitted.

A retrieval test for the reward memory were conducted 24 hours following the last conditioning session. During the test, only CS_R was presented in each trial, for a total of 20 trials. Mice were subsequently provided with free water until they were sated. This was followed by a retrieval test for the fear memory, in which only CS_P was presented in each trial, for a total of 20 trials.

Two-alternative choice (2AC) task—Mice were head-restrained with the head-bar on a home-made head-fixation system. Two metal spouts (left and right) were placed approximately 5 mm below mouse's mouth. The distance between the spouts was ~4 mm. The spouts were arranged such that the mice could reach each spout with the tongue. The spouts were made of needles (CML supply, industrial dispensing tips, 16 gauge, 1-1/2'' long) connected to silicon tubes, which were further connected to 50-ml syringes containing water or a sucrose solution. Gravity flow of liquid through the tubes was controlled by electronic valves (Lee Company, LHD series solenoid valve). The spouts were held together using a 3D printed plastic holder, which was attached to a 3-axis manual micromanipulator (Thorlabs, DT12XYZ). The placement of the spouts was adjusted with the micromanipulator, and was monitored with a webcam placed under the spouts.

Mice were kept on a water-restriction schedule (1 ml of water per day for each mouse), starting 23 h before the onset of training in the 2AC task. The training protocol for the task was derived from previous studies[54,55]. Mice were first habituated to the head-restraint frame for 10 min each day for two days. On day 3, mice were trained to lick for water from the two spouts, and were then habituated to two auditory conditioned stimuli (CS_{WA}, 10 kHz, 70dB, 1 s; CS_{SU}, 4 kHz, 70dB, 1 s) for 20 trials. 24 hours later, mice were subjected to training in the 2AC task. In each trial, the 1-s CS_{WA} or CS_{SU} was presented, followed by a 1-s delay. During the delay, mice were required to lick the left spout when hearing CS_{WA} to obtain a water reward (US_{WA}, 5 μl), and the right spout when hearing CS_{SU} to obtain a sucrose reward (US_{SU}, 5 μl, 200 mM). If mice licked the "correct" spout at least once during the delay, the trial was counted as a correct trial and mice were rewarded on that trial. If mice did not lick or lick the "wrong" spout during the delay, the trial was counted as an error trial and mice were not rewarded on that trial. Each session (1 session per day) consisted of 100 water trials and 100 sucrose trials, which were randomly interleaved and had inter-trial intervals (ITI) of 1-3 seconds. Training persisted until mice reached a performance level of at least 75% correct trials.

Go/no-go task—Mice underwent a water-deprivation schedule that started 23 h before the training and then two days of habituation to head-restraint, similar to that described in the auditory Pavlovian reward conditioning task. After the habituation, mice were trained to lick for water from a metal spout (5 μl per lick, 200 trials per session, 1 session per day for three days). Once mice have learned to successfully obtain water in at least 85% of the trials, they

were subjected to training in the "go" (or "reward-only") phase of the go/no-go task (200 trials per session, 1 session per day). In each trial, a 1-s pure tone (CS_{SU}; 10 kHz, 70dB) was presented, followed by a delay (2 s for imaging experiments and 1 s for optogenetic experiments). The delay was designated as the "decision window" during which mice were required to lick at least once in order to receive a drop of sucrose solution (US_{SU}; 10 μl, 200 mM). If mice did not lick during the decision window, they would not receive the sucrose. Training in this phase persisted until mice reached a performance level of at least 85% of successful trials.

Next, mice were trained in the final phase of the task, i.e., the go/no-go phase, which consisted of two types of trials – go trials and no-go trials. In each session (1 session per day), the two types of trials (100 go trials and 100 no-go trials) were randomly interleaved. Like the training in the "go" phase, in each of the go trials, the 1-s CS_{SU} was presented, followed by a decision window (2 s for imaging experiments and 1 s for optogenetic experiments). If mice licked at least once in the decision window, US_{SU} (10 μl) would be delivered, resulting in a "hit" trial. If mice did not lick during the window, they US_{SU} would not be delivered, resulting in a "miss" trial. In each of the no-go trials, another 1-s pure tone (CS_{QU}; 3 kHz, 70dB) was presented, followed by the decision window. If mice licked the spout at least once during the decision window, then they would receive a drop of quinine solution (US_{QU}; 10 μl, 2 mM), resulting in a "false alarm" trial. If mice did not lick during the window, they would successfully prevent quinine delivery, resulting in a "correct rejection" trial.

Two metal spouts were used next to each other in the go/no-go task to avoid mixing different solutions.

For optogenetic inhibition of US responses, laser stimulation (3-s square pulse, λ = 532 nm, 10 mW measured at the tip of optical fiber) was delivered following the onset of US presentation in each trail. For optogenetic inhibition of CS responses, the laser pulse (2 s in duration) was delivered following the onset of CS presentation in each trail. In some cases (where indicated), the laser trials (~50% of all trials) were randomly interleaved with non-laser trials.

The expected- and unexpected-reward task for dopamine neuron imaging— Mice were trained as described in the auditory Pavlovian reward conditioning task. In each trial, a 1-s CS was presented, followed by a 1-s delay and then a water reward (US; 5 μl). Once mice reached a performance level of at least 85% successful trials, they were subjected to the imaging sessions, with one session per day. Each of these sessions consisted of two types of trials: expected-reward trials in which the CS predicted the delivery of the US, and unexpected-reward trials where the US was delivered unexpectedly without the CS. Each session was composed of 100 expected-reward trials and 100 unexpected-reward trials, which were randomly interleaved.

Continuous licking task—Mice underwent a water-deprivation schedule that started 23 h before the training and then two days of habituation to head-restraint, similar to that described in the auditory Pavlovian conditioning task. As we previously described[16], after

the habituation, mice were trained to lick a metal spout for water delivery. Each lick would trigger a single opening of a water valve, calibrated to deliver 0.3 μl of water to the spout upon each opening. Mice were trained for one session per day (10 min per session) till they reached continuous licking, defined as licking the spout for 10 min without any gap longer than 10 s. Mice were tested the next day for optogenetic stimulation. During the test, laser stimulation (5-s square pulse, λ = 532 nm, 10 mW measured at the tip of optical fiber) was delivered every 40 s when mice were continuously licking. The effect of laser stimulation was calculated as: lick suppression index = $(L_{PRE} - L_{LASER}) / (L_{PRE} + L_{LASER})$, where L_{PRE} is the number of licks in the 5 s period before laser stimulation onset and L_{LASER} is the number of licks during the 5 s laser stimulation period.

Real-time place aversion or preference test

Freely moving mice were initially habituated to a two-sided chamber (23 × 33 × 25 m; made from Plexiglas) for 10 min, during which their baseline preference for the left or right side of the chamber was assessed. The test consisted of two sessions (10 min each). During the first session, we assigned one side of the chamber (counterbalanced across mice) as the photo-stimulation side, and placed the mice in the non-stimulation side to start the experiment. Once the mouse entered the stimulation side, photo-stimulation (5-ms pulses, 20 Hz, 10 mW (measured at the tip of optic fibres)), generated by a 532-nm laser (OEM Laser Systems Inc., Bluffdale, Utah, USA), was immediately turned on, and was turned off as soon as the mouse exited the stimulation side. In the second test session we repeated this procedure but assigned the other side of the chamber as the stimulation side. The behavior of the mice was videotaped with a CCD camera interfaced with Ethovision software (v11.5; Noldus Information Technologies, Leesbury, VA, USA), which was also used to control the laser stimulation and extract behavioral parameters (position, time, distance and velocity).

Behavioral data acquisition and analysis

All the behavior experiments were conducted with an open-source platform based on the Bpod State Machine (Sanworks, Rochester, NY 14604, USA). In Pavlovian reward conditioning, go/no-go task, 2AC task, and the expected- and unexpected-reward task, licking data was acquired by a custom ‘lickometer’ – a licking detection circuit that was composed of the metal spout, the mouse and a ground wire connected to the tail of the mouse. Each time mice licked the spout, the detection circuit was completed and a lick event registered. The lick events were recorded by Bpod and saved in a computer. In Pavlovian fear conditioning and imaging experiments, tail shock was generated from an isolator (ISO-Flex, A.M.P. Instruments LTD, Israel) and delivered through a pair of wires secured to the tail with silicone tubing. We tracked pupil size changes or eye blinking using an infrared-filter mounted camera (FL3-U3-13S2C-CS, Point Grey), which was controlled by an open-source Bonsai software, under lighting with infrared light-emitted diodes. Pupil or eye areas were extracted and analyzed offline by using Ethovision software (Noldus Information Technologies). The rate of changes in pupil size or eye size was processed in with custom code written in MATLAB (version 2017a; MathWorks) and was calculated as (A(t)-A0)/A0, where A(t) is the area of pupil or eye at time t, and A0 is the average area of pupil or eye.

In the 2AC task, ‘correct’ rate was calculated as the number of correct trials divided by the total trials, and ‘error’ rate was calculated as the number of error trials divided by the total trials. In the go/no-go task, ‘hit’ rate was calculated as the number of hit trials divided by the total go trials, and ‘false alarm’ rate was calculated as the number of false alarm trials divided by the total no-go trials.

In vivo calcium imaging in behaving mice

We imaged GCaMP6 signals in behaving mice using a custom-built wide-field imaging system[42-44,56]. The system consisted of four major components: excitation light source, imaging optics, CCD camera and acquisition software, and mechanical parts. An LED (470 nm; PE-100, CoolLED) was used as the excitation light source. During imaging, the light power was adjusted to 5%-10% of the maximum power based on the intensity of GcaMP6 signals.

A fluorescence illuminator (BX51, Olympus) was used to transmit light. A filter cube (U-MF2, Olympus), which contained the appropriate optical filters, was included inside the illuminator to ensure that only fluorescence signals with the desired wavelengths are transmitted. The filters used were: excitation (FF02-482/18-25, Semrock), dichroic (FF409/493/573/652-Di01, Semrock) and emission (FF01-520/35-25, Semrock). An objective lens (10x, NA 0.3, WD 11 mm; MPLFLN10X, Olympus) was used to focus the excitation light onto and collect fluorescence signals from the GRIN lens. A tube lens (180 mm; TTL180-A, Thorlabs) was paired with the objective for magnification and forming images onto a CCD camera (Retiga R3, Qimaging), which was used to collect fluorescence signals. During imaging, pixels were binned at 2 by 2 to increase frame rate and signal-to-noise ratio, and exposure time was set to 50 to 100 ms according to the intensity of GcaMP6 signals.

An acquisition software (Micro-manager, v1.4, University of California San Francisco) was used to control the camera for continuous image acquisition. During the acquisition, the camera was set to external trigger mode by the software, such that an image was captured each time the camera received a TTL signal.

An X-Y motorized stage (MMBP, Scientifica) was used to move mice around and thus adjust the positioning of the GRIN lens in the horizontal plane under the objective. A Z-motorized stage (Scientifica) was used to adjust imaging plane.

Behavior task and imaging data acquisition were synchronized through Bpod. Specifically, once a behavioral event started, Bpod would create a 5-V “start” signal and sent it to Arduino (Arduino Uno Rev3, Arduino) through a BNC cable. This signal would trigger a program written in Arduino, which would in turn command Arduino to generate a 10-Hz TTL signal. This TTL signal would be sent (via another BNC cable) to the camera, and trigger the camera to capture images at a frame rate of 10 Hz. When the behavior task ended, Bpod would set the signal back to 0 V. Consequently, the Arduino would stop generating TTL signals, and the camera would also stop capturing images.

For the imaging experiments to characterize neuronal responses to water, sucrose, food, and shock, we imaged 10 trials for water (5 μl) delivery, 10 trials for sucrose (5 μl) delivery, 5 trials for regular food pellet (20 mg) delivery, and 5 trials for tail shock (1 mA, 500 ms) delivery. To characterize neuronal responses to water (5 μl), sucrose (5 μl, 200 mM) and quinine (5 μl, 2 mM), we imaged 10 trials for each stimulus, with the delivery of the different stimuli being randomly interleaved. We subsequently imaged neuronal responses in the same mice to 5 presentations of air puff (1 s, 60 psi) and 5 presentations of tail shock (0.5 mA for 500 ms), with each of the stimuli being presented in one block. For the imaging experiments to characterize neuronal responses to regular pellets and sweet pellets, we imaged 18-24 trials for each type of pellets (20 mg), with the two types being delivered in randomly interleaved trials.

For the imaging experiments to characterize neuronal responses to both water and tail shock, we imaged 10 trials for water (5 μl) delivery and 5 trials for tail shock (0.5 mA, 500 ms) delivery. To characterize neuronal responses to different volumes (3 and 10 μl) of water, we imaged 10 trials for each volume, with the trials with different water volumes being randomly interleaved. To characterize neuronal responses to tail shocks of different intensity (0.1 and 1 mA, each for 500 ms), we imaged 5 trials for each intensity, with the trials with the same shock intensity being arranged in one block. To characterize neuronal responses to a neutral stimulus, we imaged 5 trials of neuronal responses to a 1-s pure tone (4 kHz, 70 dB).

For the imaging experiment to characterize neuronal responses during Pavlovian reward conditioning, we first imaged in naïve mice 20 trials for water delivery (US_{WA}) and 10 trials for tone presentation (CS_{WA}, 1 s, 3 kHz, 70 dB). After mice have learned the task, we imaged 20 trials of the conditioning in which both CS_{WA} and US_{WA} were presented. For the imaging experiment to characterize neuronal responses during Pavlovian aversive conditioning, we imaged 10 trials for tone presentation (CS_{SH}, 10 kHz, 70 dB) before the conditioning, and 15 trials during the conditioning in which both CS_{SH} and US_{SH} (shock) were presented. For the imaging experiment to characterize neuronal responses during retrieval, we imaged 20 trials for CS_{WA} and 20 trials for CS_{SH}. The imaging duration in each trial in these experiments was 20 s.

For the imaging experiment to characterize neuronal responses in the 2AC task, we first imaged in naïve mice 10 trials for water (US_{WA}) and sucrose (US_{SU}) delivery, and 20 trials for each CS presentation (CS_{WA}, 1 s, 10 kHz, 70 dB; CS_{SU}, 1 s, 4 kHz, 70 dB). After mice learned the task, we imaged 40 trials in the mice performing the task, with the number of water trials and sucrose trials varying from 15 to 25. The imaging duration in each trial was 14 s.

For the imaging experiment to characterize neuronal responses during the go/no-go task, we imaged once in every three trials in a session. The total number of imaging trials per session was 45, with the number of go trials and no-go trials varying from 15 to 25. The imaging duration in each trial was 18 s.

For the imaging experiments to characterize $Sst^{CeA\rightarrow DA}$ neuron responses to water, sucrose, and shock, we imaged 10 trials for water (5 μl) delivery, 10 trials for sucrose (5 μl) delivery, and 5 trials for tail shock (1 mA, 500 ms) delivery. The imaging duration in each trial was 20 s. We used two strategies to selectively label $Sst^{CeA\rightarrow DA}$ neurons with GCaMP6. First, we injected the SNc and VTA of Sst^{Cre} mice with a retrograde AAV[49,57] expressing Flp in a Cre-dependent manner (AAV8-retro-hsyn-FLEX-mTagBFP-P2A-Flp), and injected the CeA of the same mice with an AAV expressing GCaMP6 in an Flp-dependent manner (AAV-fDIO-GCaMP6). Second, as the majority of SNc- or VTA-projecting neurons in the CeL are Sst^+ (Extended Data Fig. 6c-h), we injected the SNc and VTA of wild-type mice with a retrograde AAV expressing Cre (AAV8-retro-hsyn-mTagBFP-P2A-Cre), and injected the CeL of these mice with an AAV expressing GCaMP6 in a Cre-dependent manner (AAV-DIO-GCaMP6). In both cases, we implanted a GRIN lens above the CeL for the imaging (Extended Data Fig. 7b-d). The results from these two approaches were consistent, and were thus combined for analysis.

For the experiments to characterize the dependence of dopamine (DA) neurons on Sst^+ CeA neurons, we imaged DA neuron responses before and after transient inhibition of Sst^+ CeA neurons with chemogenetics, in which we used an inhibitory DREADD derived from the kappa-opioid receptor (KORD) and applied salvinorin B (SALB) subcutaneously (s.c.; 10 mg/kg of body weight) to activate KORD[41]. As a control experiment, we imaged DA neuron responses before and after systemic application (s.c.) of DMSO (the vehicle for SALB). For the imaging experiment to characterize DA neuron responses to water, sucrose, quinine, and shock under DMSO or SALB treatment, we imaged 20 trials for water (5 μl) delivery, 20 trials for sucrose (5 μl) delivery, 7 trials for quinine (5 μl) delivery, and 10 trials for tail shock (1 mA, 500 ms) delivery. For the imaging experiment to characterize DA neuron responses during the expected- and unexpected-reward task under DMSO or SALB treatment, we imaged 20 trials for each treatment, with the number of expected reward trials and unexpected reward trials varying from 8 to 12. The imaging duration in each trial was 20 s.

Imaging data analysis

Imaging data was saved as an imaging stack in tiff format for every imaging session. The imaging stack was spatially down-sampled by a factor of 2. Margin areas in the images that didn't have any signal were cropped from the imaging stack using ImageJ (v1.51n, National Institutes of Health, USA). Motion artifacts were corrected using an algorithm for fast non-rigid motion correction (NoRMCorre) method[58]. After the correction, we applied the extended constrained non-negative matrix factorization optimized for one-photon imaging analysis (CNMF-E)[44,59,60] to demix neural signals and get their denoised and deconvolved temporal activity, termed ΔF[59,60]. We used ΔF for further analysis. The analysis with CNMF-E method was carried out using a custom MATLAB (2017a) code (see[60] for a detailed description of this method).

To determine whether a neuron was significantly ($P < 0.05$) excited or inhibited by a stimulus, and thus can be classified as being "responsive" to the stimulus, we used permutation test to compare the mean ΔF values in the 3 s immediately after stimulus

onset with those in the 3 s immediately before stimulus onset across all trials. For the different learning tasks, depending on task design, we chose the mean ΔF values in the 2-3 s immediately after CS or US onset, and the values in the 2-3 s immediately before CS onset for the comparison to determine CS- or US-responsive neurons (Pavlovian conditioning, 2.5 s; 2AC task, 2 s; go/no-go task, 3 s; expected- / unexpected-reward task, 2 s). For further analyses, such as the population analysis, we used z-scores to represent the dynamic activities in each neuron. To obtain the temporal z-scores for a neuron, we first obtained the mean activity trace for the neuron by averaging the fluorescence signals (ΔF) at each time point across all trials, and then computed the z-scores as $(F(t) - Fm) / SD$, where $F(t)$ is the ΔF value at time t, Fm and SD are the mean and standard deviation, respectively, of the ΔF values over a 2-s baseline period. For the trial-by-trial analyses, the z-scores were computed for each trial using the same method (but without the averaging across trials).

To assess the temporal relationship between the onset of behavioral response (licking and eye blinking) and the onset of neuronal response, for each neuron we calculated the z-scored ΔF at each time point, which was then averaged across all trials. For each mouse's behavioral response, we calculated the response value at each time point and averaged the values in 100-ms bins to match the imaging sampling rate (10 frames/s). The resulting values were averaged across all trials. Next, we applied the change-point analysis[44,45,61] on these data to determine the time point at which the neuronal or behavioral response significantly changed (i.e., the change-point) following the presentation of CS or US. We repeated this for all responsive neurons and calculated the difference between behavioral and neuronal change-points as the response delay of each neuron.

To analyze the trial-by-trial correlation between licking and neuronal responses, we calculated the mean licking rate and the mean ΔF value (z-scored) of each neuron during a time window t after stimulus onset in each trial (t = 2.5 s for Pavlovian conditioning, t = 3 s for memory retrieval and go/no-go task). We subsequently used these two datasets to calculate the Pearson correlation coefficient r for each neuron.

To analyze the trial-by-trial correlation between eye size changes and neuronal responses, we calculated the mean eye size change and the mean ΔF value (z-scored) of each neuron in a 3-s time window immediately after CS_P onset in each trial. We used these two datasets to calculate the Pearson correlation coefficient r for each neuron. For the time difference and correlation analyses in retrieval, we excluded the trials in which mice didn't lick or exhibit eye size change after CS onset, presumably due to extinction.

Clustering analysis—For the clustering analysis, we concatenated the trial-averaged responses (z-scores) of individual neurons to each of the stimuli, such that each row corresponds to the responses of one neuron. The responses were aligned to the onset of water or shocks. We performed principal component analysis (PCA) on the z-scores, and used principal components (PCs) for agglomerative hierarchical clustering using a correlation distance metric and complete agglomeration methods. We used the number of PCs that captured more than 80% of the variance. Pairs of neurons that were in close proximity were linked. As they were paired into binary clusters, the newly formed clusters

were grouped into larger clusters until a hierarchical tree was formed. We subsequently used the Elbow method, which calculates the within-cluster sum of squares (WCSS), to help determine the optimal number of clusters.

Cell registration—To identify the same individual cells from images acquired from different imaging sessions, we performed cell registration using a recently developed probabilistic method that automatically registers cells across multiple imaging sessions and estimates the registration confidence for each registered cell[62]. Briefly, as previously described[44], we first used the CNMF-E analysis to generate the spatial footprints for all cells imaged in an early session. We then repeated this process for the cells imaged in later sessions. We used the footprints from the early session as a reference map, and aligned with this map the footprints from the later sessions by correcting for translation and rotation differences between different sessions. We subsequently calculated the probability of a given pair of cells, each from one of two imaging sessions, to be the same cell (P_{same}) based on their spatial correlation and centroid distance. A pair of cells is considered to have the same identity if $P_{same} > 0.95$. The centroid distance between a pair of cells deemed to have the same identity is generally small (≤ 6.5 μm).

Pairwise Pearson correlation analysis—To generate the correlation coefficient matrix, we performed pairwise Pearson correlation analysis on the responses of all neurons for each stimulus pair. We first concatenated the trial-averaged responses (z-scored) of individual neurons to a stimulus, such that each row corresponds to the responses of one neuron and each dataset contains the responses of all neurons to one stimulus. The average responses in the 3-s time window immediately after stimulus onset were used for analysis. We subsequently calculated the Pearson correlation coefficient for a given pair of stimuli based on the responses of all neurons to this pair of stimuli.

Population vector analysis—To quantify the learning-induced changes in the similarity between neuronal responses at population level, we performed population vector analysis, as described previously[44,63]. Briefly, we created a series of *n*-dimensional (*n* equals the number of neurons) activity vectors for the responses (z-scored) of individual neurons at each time point. Therefore, the ensemble neuronal response at a particular time point is represented by a vector with a dimension equal to the total number of neurons in that ensemble. We used principal component analysis (PCA) for dimensionality reduction[64], and projected the population vectors onto a two-dimensional space for data visualization. To examine whether Pavlovian reward conditioning induced changes in the similarity between CS responses and US responses, for example, we computed the Mahalanobis distance (MD) between responses to CS and US[44,63], defined by:

$$MD(CS,US) = \sqrt{(PV(CS) - PV(US))^T * S^{-1}(PV(CS) - PV(US))}$$

where PV(CS) and PV(US) are the population vectors of responses to CS and US, respectively. S^{-1} is the inverse of the covariance matrix. The responses during a 2.5-s time window after CS or US onset in the Pavlovian task was used for principal component analysis (PCA) to

generate the population vectors. For the analysis on data acquired in the go/no-go task, the responses during a 3-s time window after CS or US onset was used.

Decoding analysis—We performed population decoding analysis using the linear support vector machine (SVM) in MATLAB (fitcsvm) (2017a; MathWorks) to determine whether the types of trials could be predicted on the basis of the trial-by-trial population activities of Sst^+ CeA neurons acquired in each session. We used the activities of all the simultaneously imaged neurons in each session of each mouse to perform the population decoding analysis. First, we applied principal component analysis (PCA) on the matrix of z-scored trial-by-trial neuronal activities. We used the first two PCs to represent the population activities in each trial. We subsequently used a subset of the low dimensional trial-by-trial neuronal activity data as the training dataset to train a classifier with linear kernel function ('linear') for two-class decoding (e.g., classifying water and shock trials in the Pavlovian task). Finally, we validated the classifier by using the 'predict' function to classify the trial-by-trial neuronal activities in the test dataset. Activities from randomly selected 75% of trials of each type (e.g., water and shock) were used to train the classifier, and activities from the remaining 25% of trials of each type were used to test decoding accuracy. To generate the shuffled data, we randomly reassigned a trial type to each of the trial-by-trial neuronal activities. We then followed the same procedure as that used for classifying the actual data to decode the shuffled data. We repeated this classification process 1,000 times for both the actual test dataset and the shuffled data, and calculated the average accuracy as the decoding accuracy.

Analysis of Sst$^+$ CeA neuron population dynamics in the activity space—To assess the relationship between Sst^+ CeA neuron population activity and upcoming behavioral events, we used a previously described 'coding direction' analysis[56,65-67]. For a population of n neurons, we found an $n \times 1$ vector in the n dimensional activity space that maximally separated the response vectors in go and no-go trials. We term this vector "coding direction ($\boldsymbol{cd}$)". To obtain the $\boldsymbol{cd}$, for each neuron we first computed the average z-scored response in two types of trials (e.g., hit trials and correct rejection (CR) trials), r_{hit} and r_{CR}, which are $n \times 1$ response vectors that describe the population response at each time point, t. We then computed the difference in the mean response vectors, $cd_t = r_{hit} - r_{CR}$. We averaged the values of cd_t from CS onset to US onset to obtain a single $\boldsymbol{cd}$. For a population of n neurons, this yielded an $n \times 1$ vector. The projection of population activity in hit and CR trials along the $\boldsymbol{cd}$ was obtained as $\boldsymbol{cd}^T r_{hit}$ and $\boldsymbol{cd}^T r_{CR}$, respectively. The projection along the cd captured 62 ± 6% of the total variance in Sst$^+$ CeA neuron task-related activity – which was quantified as the root mean square of the activity over the period from CS onset to US onset – in the early training stage for the hit and CR trials. It captured 63 ± 4% of the total variance in the late training stage for the hit and CR trials, and captured 57 ± 1% and 64 ± 3% of the total variance in the early and late training stages, respectively, for the hit and false alarm trials.

In vivo fiber photometry and data analysis

To record the bulk activities of dopamine neurons *in vivo* in behaving animals under head-restraint, we used a commercial fiber photometry system (Neurophotometrics Ltd., San

Diego, CA, USA) to measure GCaMP6 signals in these neurons through an optical fiber (Fiber core diameter, 200 μm; Fiber length, 5.0 mm; NA, 0.37; Inper, Hangzhou, China) implanted in the SNc or VTA. A patch cord (fiber core diameter, 200 μm; Doric Lenses) was used to connect the photometry system with the implanted optical fiber. The intensity of the blue light (λ = 470 nm) for excitation was adjusted to a low level (20~50 μW) at the tip of the patch cord. Emitted GCaMP6f fluorescence was bandpass filtered and focused on the sensor of a CCD camera. Photometry signals and behavioral events were aligned based on an analog TTL signal generated by the Bpod. Mean values of signals from a region of interest were calculated and saved by using Bonsai software (Bonsai), and were exported to MATLAB (2017a) for further analysis.

To correct for photobleaching of fluorescence signals (baseline drift), a bi-exponential curve was fit to the raw fluorescence trace and subtracted as follows:

$$F_{raw\_fit} = fit(Timestamp, F_{raw}, \text{'exp2'})$$

$$F_{raw\_correction} = \frac{F_{raw} - F_{raw\_fit}}{F_{raw\_fit}}$$

After baseline drift correction, the fluorescence signals were z-scored relative to the mean and standard deviation of the signals of the entire trace, except the time window when laser stimulation occurred (to avoid contamination by light artifact associated with the laser stimulation).

We simultaneously recorded both the calcium-dependent signals and the isosbestic signals from the GCaMP6, with the latter being excited by a 410-nm LED and serving to monitor potential motion artifacts as previously described[68]. Trials with clear motion artifacts were excluded from further analysis.

To activate Sst^+ CeA neurons with optogenetics while recording the activity of DA neurons, we delivered pulses of laser light (λ = 470 nm; pulse duration, 5 ms; frequency, 30 Hz; train duration, 200 ms; light power, 10 mw measured at the tip of optic fiber) into the CeA through an optical fiber. Another optical fiber implanted in the ipsilateral SNc or VTA was used for measuring DA neuron activity with photometry. Mice under water restriction were trained to lick a metal spout to get water reward. Laser stimulation trials and water-reward trials were randomly interleaved, with 60-s inter-trial intervals. Photometry signals and licking events in the 2-s time windows immediately before and after the onset of laser stimulation, or water delivery, were used for further data analysis.

Statistical analysis

All statistics are indicated where used. Statistical analyses were conducted using GraphPad Prism Software (v7; GraphPad Software, Inc., La Jolla, CA) and MATLAB (2017a) statistical toolbox (MathWorks). To determine whether parametric tests could be used, the D'Agostino-Pearson Test or Shapiro-Wilk Test was performed on all data as a test for normality. The statistical test used for each comparison is indicated when used. Parametric

tests were used whenever possible to test differences between two or more means. Non-parametric tests were used when data distributions were non-normal. Analysis of variance (ANOVA) was used to check for main effects and interactions in experiments with repeated measures and more than one factor. When main effects or interactions were significant, we did the planned comparisons according to experimental design (for example, comparing laser on and off conditions). All comparisons were two tailed. Statistic hypothesis testing was conducted at a significance level of 0.05.

Extended Data

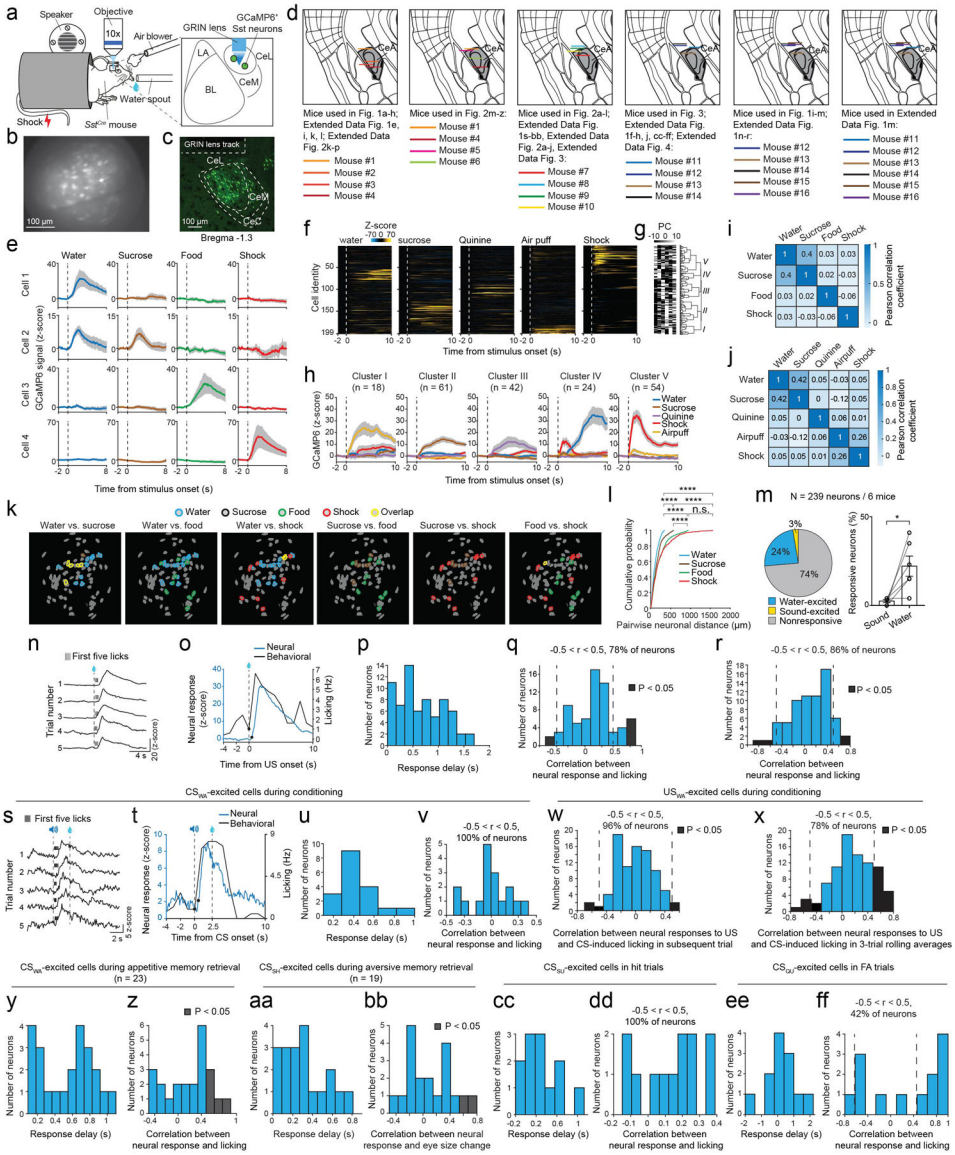

Extended Data Figure 1 |. Characterization of Sst^{+} CeA neuronal responses.

a, A schematic of the experimental setup and the approach. **b**, A raw image of the field of view under a GRIN lens. **c**, A confocal histological image of a coronal brain section from a representative mouse used for the imaging experiments, showing GCaMP6 expression

in Sst^+ CeA neurons and the location of GRIN lens implantation. **d**, Schematics showing the placement of GRIN lens implants in the mice (n = 16 mice) used for the imaging experiments. Note that some mice were used in more than one experiment, as indicated. **e**, Four example neurons showing selective responses to different stimuli. **f**, Heat-maps of the responses of all neurons to different stimuli. Each row represents the activities of one neuron. **g**, The first six principle components (PC) (explain 84% of the variance) and hierarchical clustering dendrogram showing the relationship of each neuron within the five clusters. **h**, Average responses of each cluster to different stimuli (n = 199 neurons/4 mice). **i & j**, Correlation coefficient matrixes of the responses of all neurons for each stimulus pair. **k**, The spatial locations of individual extracted neurons in the field of view (FOV) in the CeA of a representative mouse. Sst^+ neurons excited by different stimuli are color coded. **l**, Cumulative probability distributions of the pairwise distances (measured as centroid distances) of neurons excited by different stimuli, as indicated, in the FOV. The distributions of the pairwise distances were significantly different between groups (water-excited neurons vs. sucrose-excited neurons, ****P = 1.33e-04; water-excited neurons vs. food-excited neurons, ****P = 1.06e-12; water-excited neurons vs. shock-excited neurons, ****P = 6.28e-13; sucrose-excited neurons vs. food-excited neurons, ****P = 1.39e-05; sucrose-excited neurons vs. shock-excited neurons, ****P = 2.40e-06; food-excited neurons vs. shock-excited neurons, n.s., nonsignificant, P = 0.34; Kolmogorov-Smirnov test). Data from 4 mice were pooled together (n = 243 cells/4 mice). **m**, Left: pie chart of the percentage distributions of Sst^+ CeA neurons in naïve mice, showing those selectively excited by water or sound, or neither stimulus (nonresponsive). Right: the fractions of sound- or water-excited neurons in individual mice (n = 239 neurons/6 mice, *P = 0.0224, paired t-test). Sound intensity, 70 dB. **n**, Trial-by-trial activities of a representative water-excited neuron and the first 5 licking responses of the mouse in response to water delivery. Both the neural and the licking responses are aligned to the onset of water presentation (dashed line). **o**, The timing of increase in activity in the water-excited neuron shown in n, and the timing of increase in licking response of the corresponding mouse after the onset of water delivery, as determined by change-point analysis (Methods). Black dots represent the change-points. **p**, Quantification of the difference between neural and behavioral change-points, for all water-excited neurons and the corresponding mice. Values above zero indicate that neural responses lag behind behavioral responses. **q & r**, Histogram showing the distribution of water-excited neurons based on the trial-by-trial Pearson correlation coefficients between their activities and the licking rates of the mouse in the 3-s (q) or 10-s (r) time window immediately after the onset of water delivery (n =10, r (8) = 0.64, P = 0.046; P > 0.05 when $-0.64 < r < 0.64$; t-test). **s-x,** Data acquired during the conditioning phase. **s,** Trial-by-trial activities of a representative CS_{WA}-excited neuron and the first 5 licking responses of the mouse in response to CS_{WA}. Both the neural and the licking responses are aligned to CS_{WA} onset. **t**, The timing of increase in activity in the neuron shown in s, and the timing of increase in licking response of the corresponding mouse after CS_{WA} onset, as determined by change-point analysis (Methods). Black dots represent the change-points. **u**, Quantification of the difference between neural and behavioral change-points, for all the responsive neurons and the corresponding mice. Values above zero indicate that neural responses lag behind behavioral responses. **v**, Histogram showing the distribution of neurons based on trial-by-trial Pearson correlation coefficients between their average activities and the licking

rates of the mouse in the 2.5-s time window immediately after CS_{WA} onset. **w**, Histogram showing the distribution of neurons based on Pearson correlation coefficients between their US_{WA} responses and the CS_{WA}-induced licking rates of the mouse in subsequent trials (n = 19, r(17) = 0.46, P = 0.047; P > 0.05 when −0.46 < r < 0.46; t-test). **x**, Histogram showing the distribution of neurons based on Pearson correlation coefficients between their US_{WA} responses (in three-trial rolling averages) and the CS_{WA}-induced licking rates of the mouse (in the corresponding three-trial rolling averages) (n = 18, r(16) = 0.47, P = 0.049; P > 0.05 when −0.47 < r < 0.47; t-test). **y-bb**, Data acquired during the retrieval phase. **y**, Quantification of the difference between neural and behavioral change-points, for all the neurons excited by CS_{WA} and the corresponding mice. **z**, Histogram showing the distribution of neurons based on trial-by-trial Pearson correlation coefficients between their average activities and the licking rates of the mouse in the 3-s time window immediately after CS_{WA} onset (n = 20, r(18) = 0.45, P = 0.046; P > 0.05 when −0.45 < r < 0.45; t-test). **aa**, Quantification of the difference between neural and behavioral change-points, for all the neurons excited by CS_{SH} and the corresponding mice. **bb**, Histogram showing the distribution of neurons based on trial-by-trial Pearson correlation coefficients between their average activities and the eye size change of the mouse in the 3-s time window immediately after CS_{SH} onset (n = 15, r(13) = 0.52, P = 0.047; P > 0.05 when −0.52 < r < 0.52; t-test). **cc-ff,** data from the go/no-go task. **cc**, Quantification of the difference between neural and behavioral change-points, for all the neurons excited by CS_{SU} and the corresponding mice in hit trials. **dd**, Histogram showing the distribution of neurons based on trial-by-trial Pearson correlation coefficients between their average activities and the licking rates of the mouse in the 3-s time window immediately after CS_{SU} onset. **ee**, Quantification of the difference between neural and behavioral change-points, for all the neurons excited by CS_{QU} and the corresponding mice in false alarm (FA) trials. **ff**, Histogram showing the distribution of neurons based on trial-by-trial Pearson correlation coefficients between their average activities and the licking rates of the mouse in the 3-s time window immediately after CS_{QU} onset.

Data are presented as mean ± s.e.m. Shaded areas represent s.e.m.

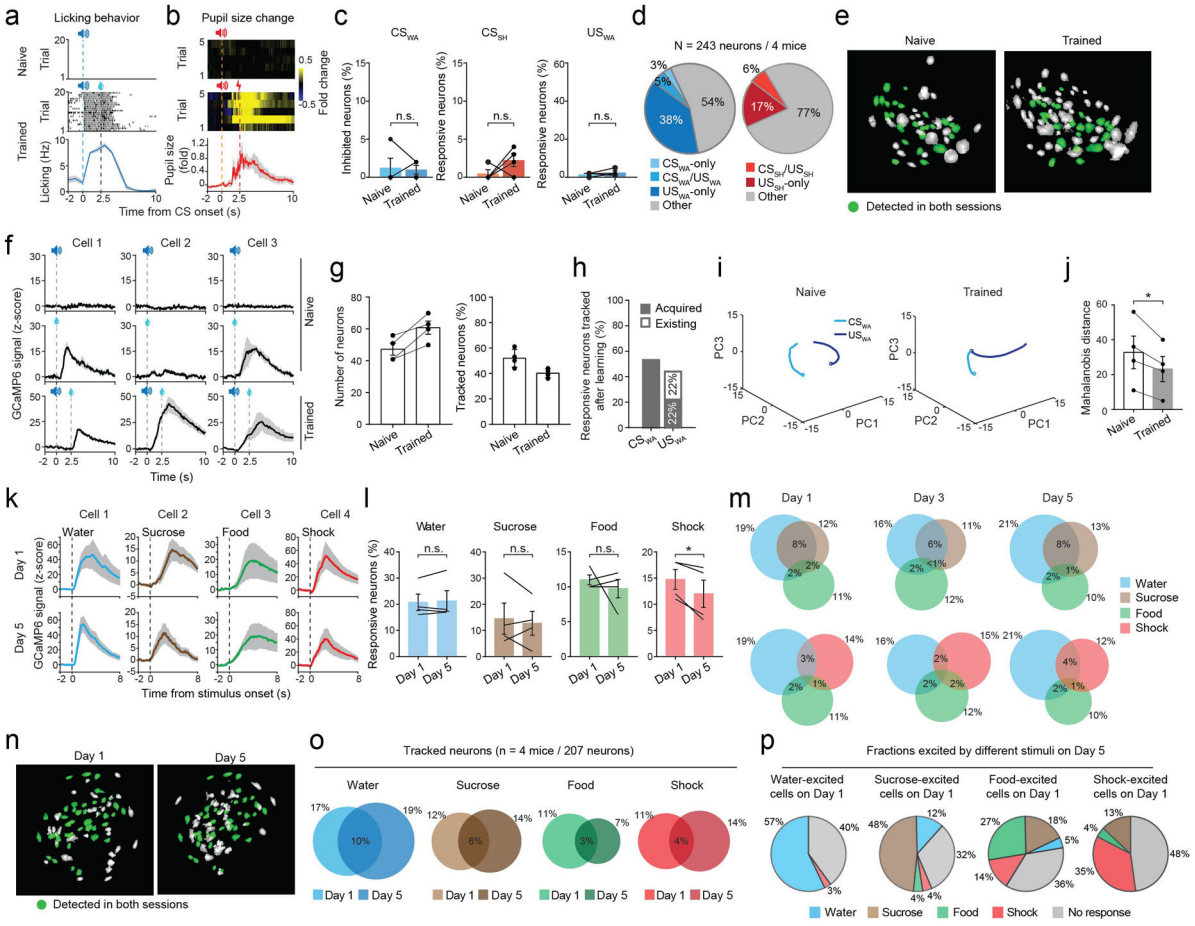

Extended Data Figure 2 |. Imaging Sst$^+$ CeA neuron activities with or without learning.
a, Top and middle panels: trial-by-trial licking events for a representative mouse in response to a sound in naïve state (top), and in response to the sound (CS_{WA}) and water (US_{WA}) after training in the Pavlovian reward conditioning (middle). Bottom: average licking rate across trials for this mouse after training. **b**, Top and middle panels: trial-by-trial pupil size change for a representative mouse in response to a sound before training (top), and in response to the sound (CS_{SH}) and shock (US_{SH}) after training in the Pavlovian fear conditioning (middle). Bottom: average pupil size change across trials for this mouse after training. **c**, Quantification of the percentage of Sst$^+$ CeA neurons showing inhibitory responses to different stimuli before and after training (n = 4 mice; CS_{WA}, P = 0.8240, US_{WA}, P = 0.3534, CS_{SH}, P = 0.2754; n.s., nonsignificant, paired t-test). **d**, Pie charts showing the percentage distributions of Sst$^+$ CeA neurons according to their response profiles to CS and US after training in reward conditioning (left) or fear conditioning (right). **e**, Footprints of Sst$^+$ CeA neurons in a representative mouse imaged at naïve (left) stage and after training (right). After image alignment, the neurons detected in both sessions are labelled in green. **f**, Average activity traces of three example tracked neurons in different types of trials at naïve stage (upper two rows) and after training (bottom row). **g**, Left, the number of neurons detected at different training stages across mice. Right, the percentage of tracked neurons at different training stages across mice (n = 4 mice). **h**, Quantification of the percentage

of tracked neurons among the CS_{WA}- or US_{WA}-responsive neurons in trained mice. Note that all the CS_{WA}-responsive neurons were newly acquired during training; by contrast, 50% of the US_{WA}-responsive neurons were newly acquired during training, and the other 50% of these neurons existed at the naïve stage. **i**, The population activities of tracked neurons in one representative mouse in response to CS_{WA} and US_{WA} at naïve stage (left) and after training (right). The first three principal components of the population activities are projected onto a 3D space. **j**, Quantification of the Mahalanobis distance between the vector representing CS_{WA} responses and that representing US_{WA} responses across training stages (n = 4 mice; *P = 0.0267, paired t-test). **k-p,** Tracking Sst^+ CeA neuron activities across days without learning. **k**, Four example neurons showed stable responses to water, sucrose, food, or shock on day 1 and day 5. **l**, Percentage of responsive neurons to each stimulus across mice on day 1 and day 5 (n = 4 mice; water, P = 0.6376; sucrose, P = 0.6139; food, P = 0.5636; shock, *P = 0.0486; n.s., nonsignificant; paired t-test). **m**, Percentage distributions of neurons excited by different stimuli on day 1, day 3 and day 5 (Fisher's exact test on the overlaps, water/sucrose: day 1, ****P = 4.28e-13, day 3, ****P < 1e-15, day 5, ****P = 4.09e-11; water/food: day 1, P = 0.3818, day 3, P = 0.1163, day 5, P = 0.1362; water/shock: day 1, P = 0.5178, day 3, P > 0.9999, day 5, P = 0.5527; sucrose/food: day 1, P = 0.2684, day 3, P = 0.2823, day 5, P = 0.8011; food/shock: day 1, P = 0.4434, day 3, P = 0.6465, day 5, P > 0.9999). **n**, Footprints of Sst^+ CeA neurons in a representative mouse imaged on day 1 (left) and day 5 (right). After image alignment, the neurons detected in both sessions are labelled in green. **o**, Neurons were tracked across day 1 and day 5. Each Venn diagram shows the relationship between the neurons excited by a stimulus on day 1 and those excited by the same stimulus on day 5 (Fisher's exact test on the overlaps: water, ****P = 2.32e-09; sucrose, ****P = 5.36e-06; food, **P = 0.0016; shock, **P = 0.0014). The percentage distributions are calculated based on all the tracked neurons (207 neurons in 4 mice). **p**, Each pie chart shows, for the neurons excited by a stimulus on day 1, the fractions of these neurons excited by other stimuli on day 5.

Data are presented as mean ± s.e.m. Shaded areas represent s.e.m.

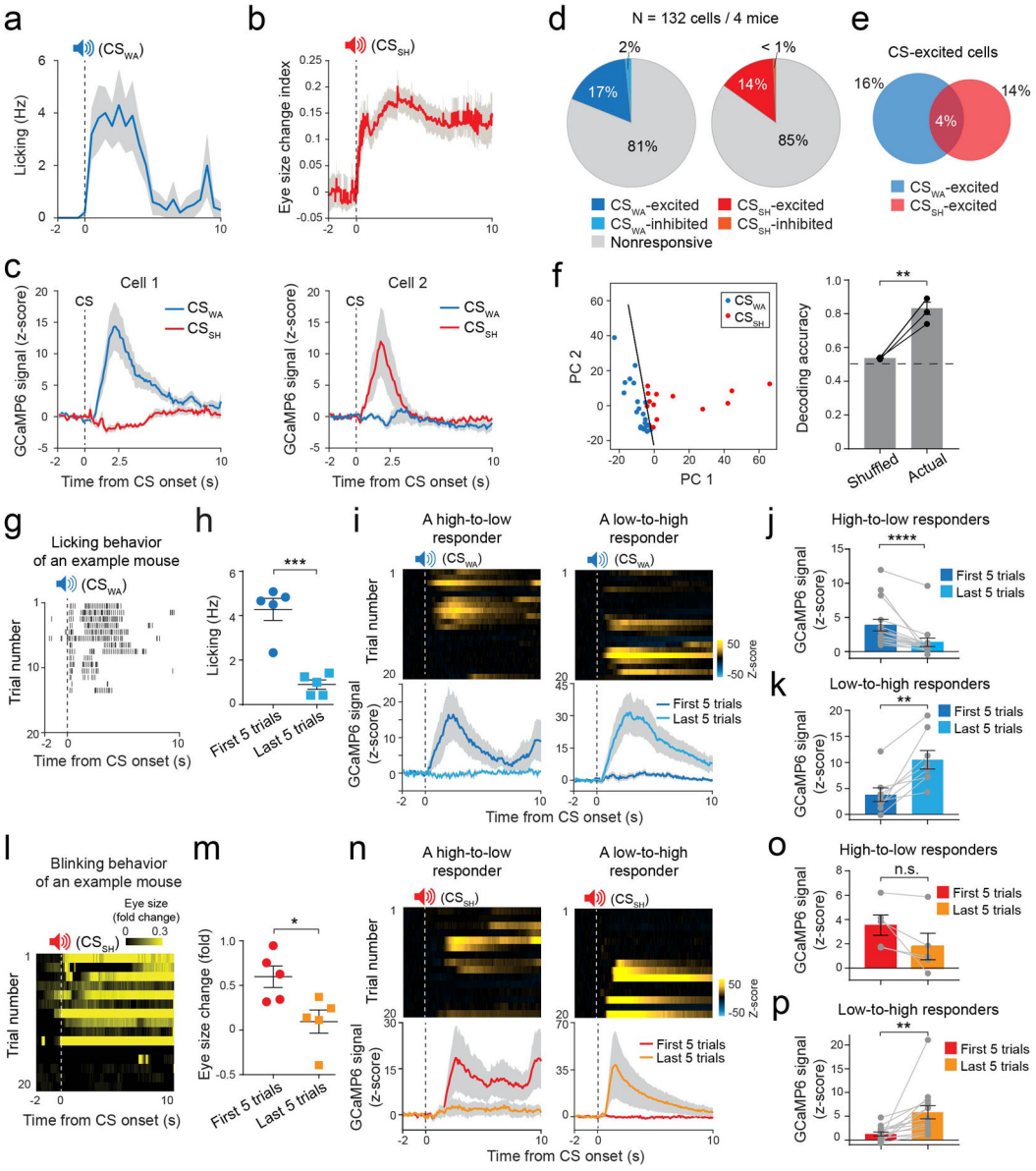

Extended Data Figure 3 |. Stimulus-specific responses in Sst$^+$ CeA neurons during the retrieval of appetitive and aversive memories.

a, Average licking rate of a representative mouse in response to CS_{WA} in the retrieval test. **b**, Average eye size change in a representative mouse in response to CS_{SH} in the retrieval test. **c**, Two example Sst$^+$ CeA neurons exhibiting different responses to CS_{WA} and CS_{SH} in the retrieval test. **d**, Pie charts showing the percentage distributions of Sst$^+$ CeA neurons according to their response profiles to the CS in the retrieval test for the appetitive (left) or fear memory (right). **e**, Percentage distributions of the neurons excited by CS_{WA}, CS_{SH}, or both stimuli (overlap) in the retrieval test (Fisher's exact test on the overlap: P = 0.1821). **f**, Left, an example of SVM decoding using the principal components (PC) of Sst$^+$ CeA population activities in response to CS_{WA} and CS_{SH} in the retrieval test. Right, performance of the decoding as shown in the left. Actual, decoding analysis using the actual responses of neurons to CS_{WA} and CS_{SH}; shuffle, decoding analysis using the responses of neurons that

were shuffled across trial types (n = 4 mice, **P = 0.0037, paired t-test). **g**, Trial-by-trial licking events for a representative mouse in response to CS_{WA} during the retrieval test. **h**, Average licking rate in early trials was higher than late trials during retrieval of the appetitive memory (n = 4 mice, ***P = 0.0002, t-test). **i**, Top: trial-by-trial responses of two example neurons to CS_{WA}. Bottom, average responses of the respective neurons on the top, for the first 5 and last 5 trials during the retrial test. **j** & **k**, Quantification of the CS_{WA} responses for neurons showing higher (j) or lower response (k) to CS_{WA} in the first 5 trials than the last 5 trials in the retrieval test (n = 15 neurons, ****P = 6.10e-05, Wilcoxon matched-pairs signed rank test; n = 8 neurons, **P = 0.003, paired t-test). **l**, Trial-by-trial blinking behavior for a representative mouse in response to CS_{SH} during the retrieval test. **m**, Average eye size change in early trials was higher than late trials during retrieval of the fear memory (n = 4 mice, *P = 0.0219, t-test). **n**, Top: trial-by-trial responses of two example neurons to CS_{SH}. Bottom, average responses of the respective neurons on the top, for the first 5 and last 5 trials during the retrial test. **o** & **p**, Quantification of the CS_{SH} responses for neurons showing higher (o) or lower response (p) to CS_{SH} in the first 5 trials than the last 5 trials in the retrieval test (n = 5 neurons, n.s., nonsignificant, P = 0.0823; n = 14 neurons, **P = 0.008, paired t-test).

Data are presented as mean ± s.e.m. Shaded areas represent s.e.m.

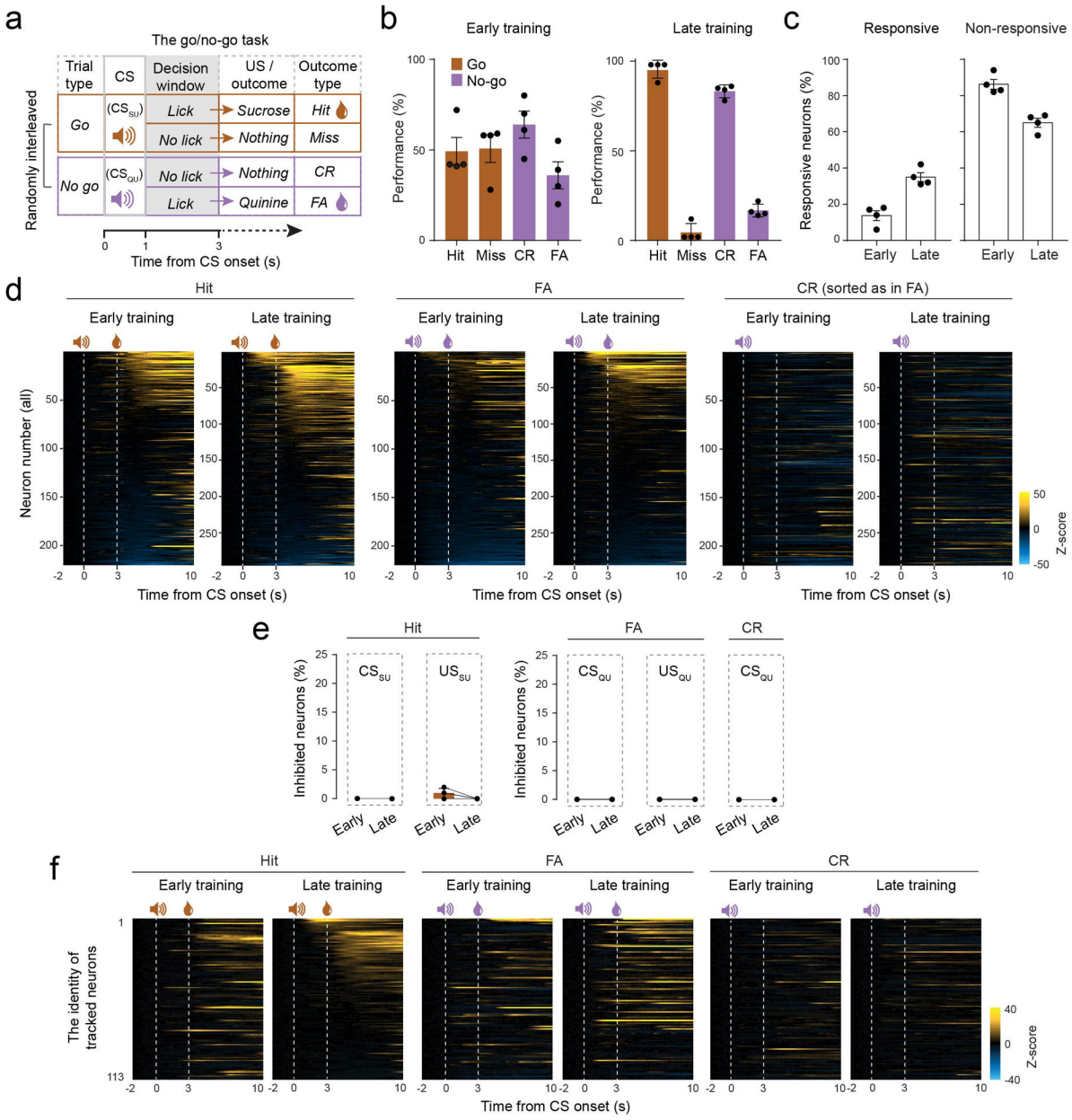

Extended Data Figure 4 |. Imaging Sst^{+} CeA neuron activities in the go/no-go task.

a, A schematic of the go/no-go task design. **b**, Performance of mice (n = 4 mice) in the go/no-go task at the early and late training stages. **c**, Percentage of responsive and non-responsive neurons imaged at the early and late training stages (n = 4 mice). **d**, Heat-maps of the activities of all neurons in different trial types at the early and late training stages. Each row in each panel represents the activities of one neuron. Neurons in each panel are sorted based first on the response to CS and subsequently on the response to US. Neurons in CR trials are sorted in the same order as that in FA trials. **e**, Quantification of the fractions of neurons showing inhibitory responses in different trial types at different stages of training (n = 4 mice). **f**, Heat-maps of the activities of all tracked neurons in different trial types at the

early and late training stages. Each row represents the activities of one neuron. All neurons are sorted based on the responses in the late training stage in Hit trials.
Data in b, c, e are presented as mean ± s.e.m.

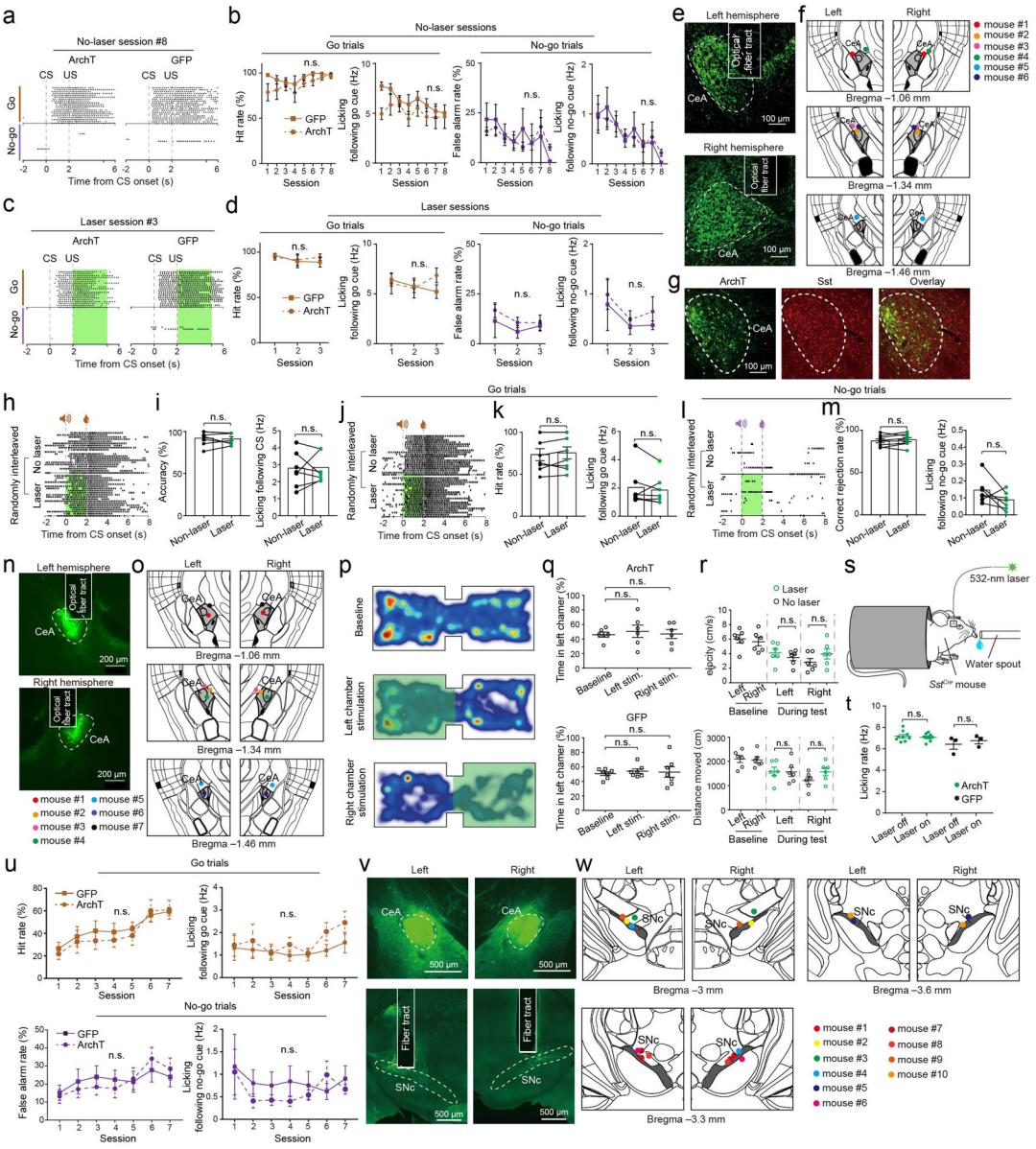

Extended Data Figure 5 |. Control experiments for optogenetic manipulation.

a-g, Optogenetic inhibition of Sst^{+} CeA neurons during US presentation in well-trained mice does not impair performance. **a**, A representative ArchT mouse (left) and GFP mouse (right) used in Figure 4 was given additional 8 sessions of training in the go/no-go task in the absence of laser stimulation. The licking events, sorted according to trial types, for the two mice in session 8 (S8) of the additional training, in which they have reached similar levels of performance and anticipatory licking. **b**, All the mice used in Figure 4 were given additional 8 sessions of training in the go/no-go task in the absence of laser

stimulation. Their performance and anticipatory licking rate in different sessions and trial types were quantified (ArchT group, n = 6 mice, GFP group, n = 5 mice; last session, n.s., nonsignificant, P > 0.05; t-test). **c** & **d**, The same mice as in b were tested in another 3 sessions, in which the laser stimulation was delivered to the CeA immediately following the onset of US delivery in each trial. **c**, Behavior of a representative ArchT mouse (left) and GFP mouse (right) in the 3rd of the test sessions. The licking events were sorted according to trial types. Dashed lines indicate the onset of CS and US. The green shaded area indicates the time window in a trial when the laser was turned on. **d**, Behavior of all the mice across sessions during the test. Their performance and anticipatory licking rate in different sessions and trial types were quantified (n.s., P > 0.05; two-way ANOVA). **e**, Confocal histological images of coronal brain sections from a representative mouse used for the experiments, showing ArchT-GFP expression in Sst$^+$ CeA neurons and the locations of optical fiber implantation. **f**, Schematics showing the placement of fiber implants in the ArchT mice (n = 6 mice) used for the experiments. **g**, Confocal histological images of a coronal brain section from a representative mouse, showing ArchT-GFP expression (left) and the expression of Sst recognized by an antibody (middle). Almost all ArchT-GFP$^+$ cells are also Sst$^+$ (right). **h-o,** Optogenetic inhibition of Sst$^+$ CeA neurons during CS presentation in well-trained mice does not impair performance. **h** & **i**, Behavior of well-trained ArchT mice in the reward-only task. **h**, The licking events of a representative mouse sorted according to laser and no-laser trials. Dashed lines indicate the onset of CS and US. The green shaded area (2 s) indicates the time window in a trial when the laser was turned on (50% of trials). **i**, The performance (left) and anticipatory licking rate (right) of all the mice in laser and no-laser trials (n = 7 mice, n.s., nonsignificant, P > 0.05; paired t-test). **j** & **k**, Behavior of the same mice in i after being well trained in the go/no-go task. **j**, The licking events of a representative mouse sorted according to laser and no-laser trials in the go trials. Dashed lines indicate the onset of CS and US. The green shaded area (2 s) indicates the time window in a trial when the laser was turned on (50% of go trials). **k**, The performance (left) and anticipatory licking rate (right) of all the mice in laser and no-laser trials (n.s., P > 0.05; paired t-test). **l** & **m**, Same as j & k, except that the no-go trials are used for the presentation (l) and analyses (m) (n.s., P > 0.05; paired t-test). **n**, Histological images of coronal brain sections from a representative mouse used for the experiments, showing ArchT-GFP expression in Sst$^+$ CeA neurons and the locations of optical fiber implantation. **o**, Schematics showing the placement of fiber implants in the ArchT mice (n = 7 mice) used for the experiments. **p-t,** Optogenetic inhibition of Sst$^+$ CeA neurons does not induce aversion or preference and has no effect on movements. **p**, Heat-maps for the activity of a representative ArchT mouse at baseline (top), or in a situation whereby entering the left (middle) or right (bottom) side of the chamber triggered photo-inhibition of Sst$^+$ CeA neurons (i.e., the real-time place preference/aversion (RTPP/RTPA) test). **q**, Quantification of the behavior as shown in a, for mice in which Sst$^+$ CeA neurons expressed ArchT (n = 6 mice, top) or GFP (n = 7 mice, bottom) (n.s., nonsignificant), P > 0.05, one-way ANOVA. **r**, Quantification of moving velocity (top) and distance (bottom) for the ArchT mice in q in the RTPP/RTPA test (n.s., P > 0.05, one-way ANOVA). **s** & **t**, Experiment with the continuous licking task. **s**, A schematic of the setup for the task. **t**, Quantification of the effect of laser stimulation on licking rate in ArchT mice and GFP mice (n.s., P > 0.05, one-way ANOVA). **u-w,** Optogenetic inhibition of Sst$^{CeA\rightarrow DA}$ projections in the go/no-go task after mice learned the reward task. The same mice used in

Figure 5b were further trained in the absence of laser stimulation such that the ArchT group and GFP group reached similar performance in the reward-only task. The two groups were subsequently trained in the go/no-go task, during which a green light (3 s) was delivered into the CeA immediately after the onset of US presentation in each trial throughout the training. **u,** Top left, hit rate across training sessions (ArchT group, n = 10 mice, GFP group, n = 11 mice; $F(1,19) = 0.1965$, n.s., nonsignificant, $P = 0.6626$; two-way ANOVA). Top right, licking rate following CS onset in go trials across training sessions ($F(1,19) = 0.4038$, n.s., $P = 0.5327$; two-way ANOVA). Bottom left, false alarm rate across training sessions ($F(1,19) = 0.1985$, n.s., $P = 0.6610$; two-way ANOVA). Bottom right, licking rate following CS onset in no-go trials across training sessions ($F(1,19) = 0.7804$, n.s., $P = 0.388$; two-way ANOVA). **v**, Histological images of coronal brain sections from a representative mouse used for the experiments, showing ArchT-GFP expression in Sst^+ CeA neurons (top) and the locations of optical fiber implantation in the SNc (bottom). **w**, Schematics showing the placement of fiber implants in the SNc of the ArchT mice used for the experiment.
Data are presented as mean ± s.e.m.

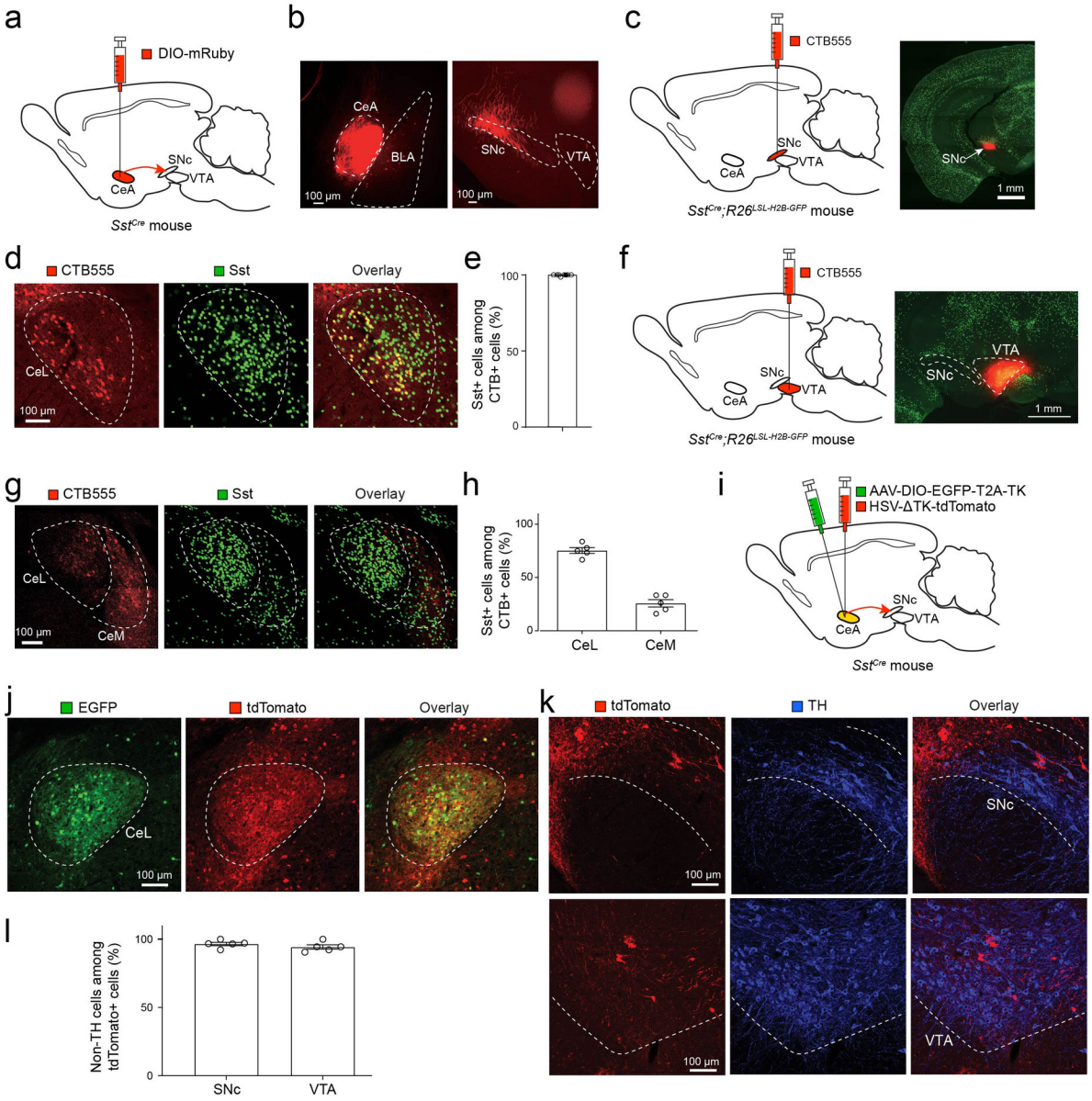

Extended Data Figure 6 l. The $Sst^{CeA \rightarrow DA}$ projections.

a, A schematic of the approach. **b**, Images of the expression of the red fluorescent protein mRuby in Sst^+ CeA neurons (left) and their projections to the SNc (right) in a representative Sst^{Cre} mouse as prepared in a. **c**, A schematic of retrograde tracing with CTB injection into the SNc (left), and an image showing the injection in a representative $Sst^{Cre};R26^{LSL\text{-}H2B\text{-}GFP}$ mouse (right). **d**, Confocal images showing the CTB labelled neurons (left), Sst^+ neurons (middle), and their overlap in the CeA (right). **e**, Quantification of the Sst^+ neurons among CTB-labelled neurons in the CeA (n = 8 mice). **f, g & h**, Same as c, d & e, respectively, except that CTB was injected into the VTA (n = 5 mice). CeL, lateral subdivision of the CeA; CeM, medial subdivision of the CeA. **i**, A schematic of the approach for anterograde transsynaptic tracing of Sst^+ CeA neurons. **j**, Confocal images showing CeA neurons infected by AAV-DIO-EGFP-T2A-TK (left) and HSV-ΔTK-tdTomato (middle), which are

the two components of the anterograde transsynaptic tracing system. The “starter cells” are the neurons infected by both viruses (i.e., the yellow cells on the right). **k**, Confocal images showing the postsynaptic cells labelled by HSV-ΔTK-tdTomato (left panels), which are located in the SNc (top panels) and VTA (bottom panels). The DA neuronal marker tyrosine hydroxylase (TH) was recognized by an antibody (middle panels). Almost none of the HSV-labelled (tdTomato^{+}) neurons expressed TH (right panels). **l**, Quantification of the non-TH cells (which are putative GABAergic neurons) among all the tdTomato^{+} neurons in the SNc and VTA (n = 5 mice).

Data are presented as mean ± s.e.m.

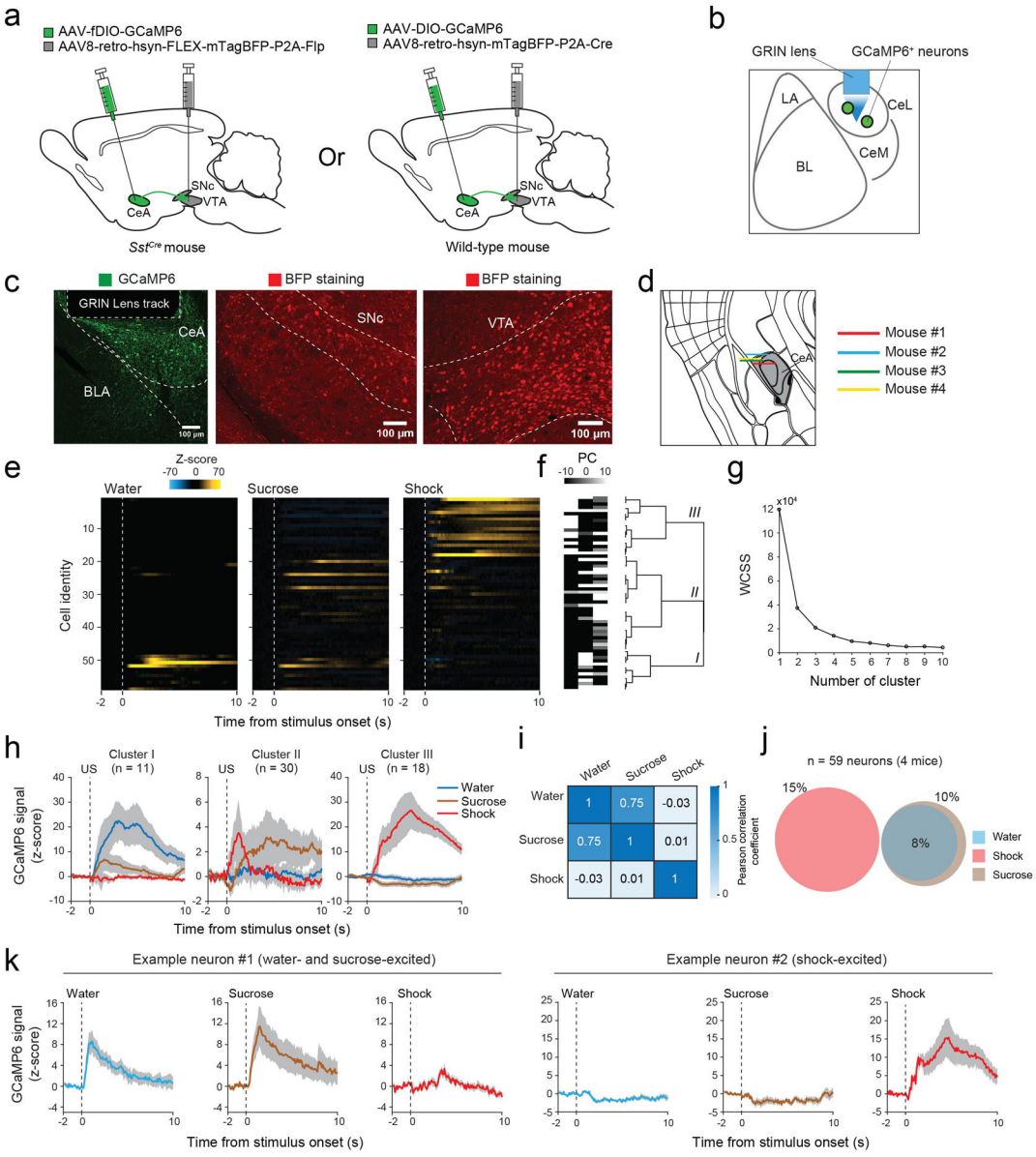

Extended Data Figure 7 l. Imaging Sst$^{CeA\rightarrow DA}$ neurons.

a, Schematics of the approach to label $Sst^{CeA\rightarrow DA}$ neurons with GCaMP6. **b**, A schematic of the approach for imaging. **c**, Confocal histological images of coronal brain sections from a representative mouse used for the experiment. Left: expression of GCaMP6 in $Sst^{CeA\rightarrow DA}$ neurons and the locations of GRIN Lens implantation. Middle and right: infection of neurons in the SNc (middle) and VTA (right) by the AAV8-retro-hsyn-mTagBFP-P2A-Cre, as indicated by the expression of BFP. **d**, Schematics showing the placement of GRIN lens implants in the mice (n = 4 mice) used for the experiment. **e**, Heat-maps of the responses of all neurons to different stimuli. Each row represents the activities of one neuron. **f**, The first three principle components (PC) (explain 82% of the variance) and hierarchical clustering dendrogram showing the relationship of each neuron within the three clusters. **g**, Quantification of the within-cluster sum of squares (WCSS) in f. **h**, Average responses of each cluster to different stimuli (n = 59 neurons/4 mice). **i**, Correlation coefficient matrix of the responses of all neurons for each stimulus pair. **j**, Percentage distributions of neurons excited by different stimuli (Fisher's exact test on the overlaps: water/sucrose, ****P = 1.20e-06; water/shock, P > 0.9999; sucrose/shock, P = 0.5768). **k**, The responses of two example $Sst^{CeA\rightarrow DA}$ neurons to different stimuli.
Data are presented as mean ± s.e.m. Shaded areas represent s.e.m.

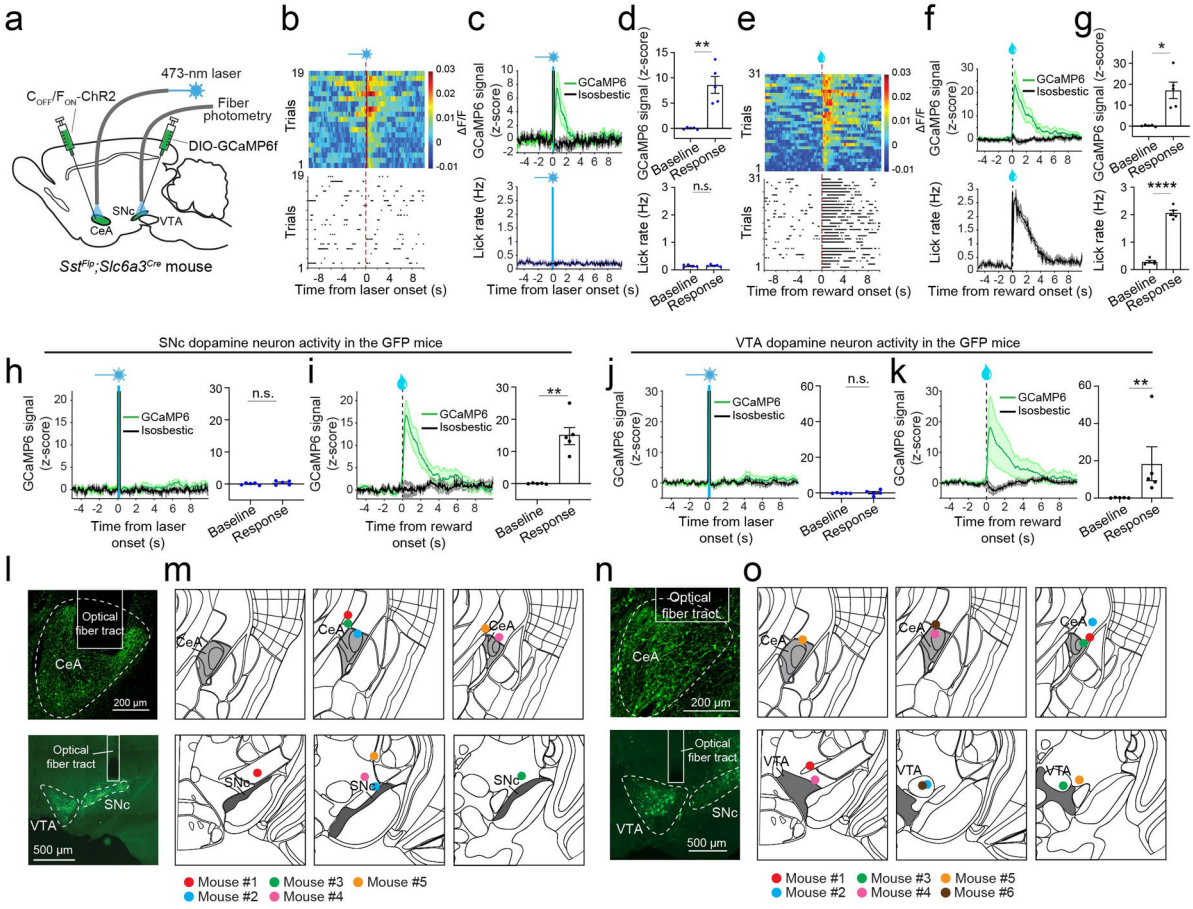

Extended Data Figure 8 l. Activation of Sst^{+} CeA neurons promotes DA neuron activity.

a, A schematic of the approach to record SNc DA neuron activity while activating Sst^+ CeA neurons. **b**, Top: trial-by-trial activity heat-maps of SNc DA neurons in one mouse, showing the responses induced by optogenetic activation of Sst^+ CeA neurons. Bottom: trial-by-trial licking events from the same mouse. **c**, Top: calcium-dependent (green) and the simultaneously recorded isosbestic (black) GCaMP6 fluorescence signals in SNc DA neurons of the mouse in b. Bottom: average licking rate of the mouse. Blue bars represent laser stimulation (200 ms) in the CeA. **d**, Quantification of average neural activities (top) and licking rate (bottom) in 2-s time windows immediately before ("baseline") and after ("response") the laser stimulation (n = 5 mice; top, **P = 0.0066; bottom, n.s., nonsignificant, P = 0.1778; paired t-test). **e, f & g**, same as b, c & d, respectively, except that water was given to mice instead of optogenetic stimulation in the CeA (quantification in g: n = 5 mice; top, *P = 0.0121; bottom, ****P =3.38e-05; paired t-test). **h & i**, SNc DA neuron activity in the GFP control mice. **h**, Left: calcium-dependent (green) and the simultaneously recorded isosbestic (black) GCaMP6 fluorescence signals in SNc DA neurons of a mouse. Right: quantification of average neural activities in 2-s time windows immediately before ("baseline") and after ("response") the laser stimulation (n = 5 mice, n.s., P = 0.3065; paired t-test). **i**, same as h, except that water was given to mice instead of optogenetic stimulation in the CeA (n = 5 mice, **P = 0.0046; paired t-test). **j & k**, same as h & i, respectively, except that VTA DA neuron activity was recorded. **j**, Quantification: n = 5 mice, n.s., P = 0.6973; paired t-test. **k**, Quantification: n = 5 mice, **P = 0.0079; Mann-Whitney test. **l-o,** Histology of the mice. **l,** Histological images of coronal brain sections from a representative mouse, showing ChR2-eYFP expression in Sst^+ CeA neurons and the location of optical fiber implantation in the CeA (top), as well as GCaMP6 expression in SNc DA neurons and the location of optical fiber implantation in the SNc (bottom). **m**, Schematics showing the placement of fiber implants in the CeA for optogenetic stimulation (top), and in the SNc of the same mice for photometry (bottom) (n = 5 mice). **n & o,** same as l & m, respectively, except that photometry recording was performed in the VTA (n = 6 mice).
Data are presented as mean ± s.e.m. Shaded areas represent s.e.m.

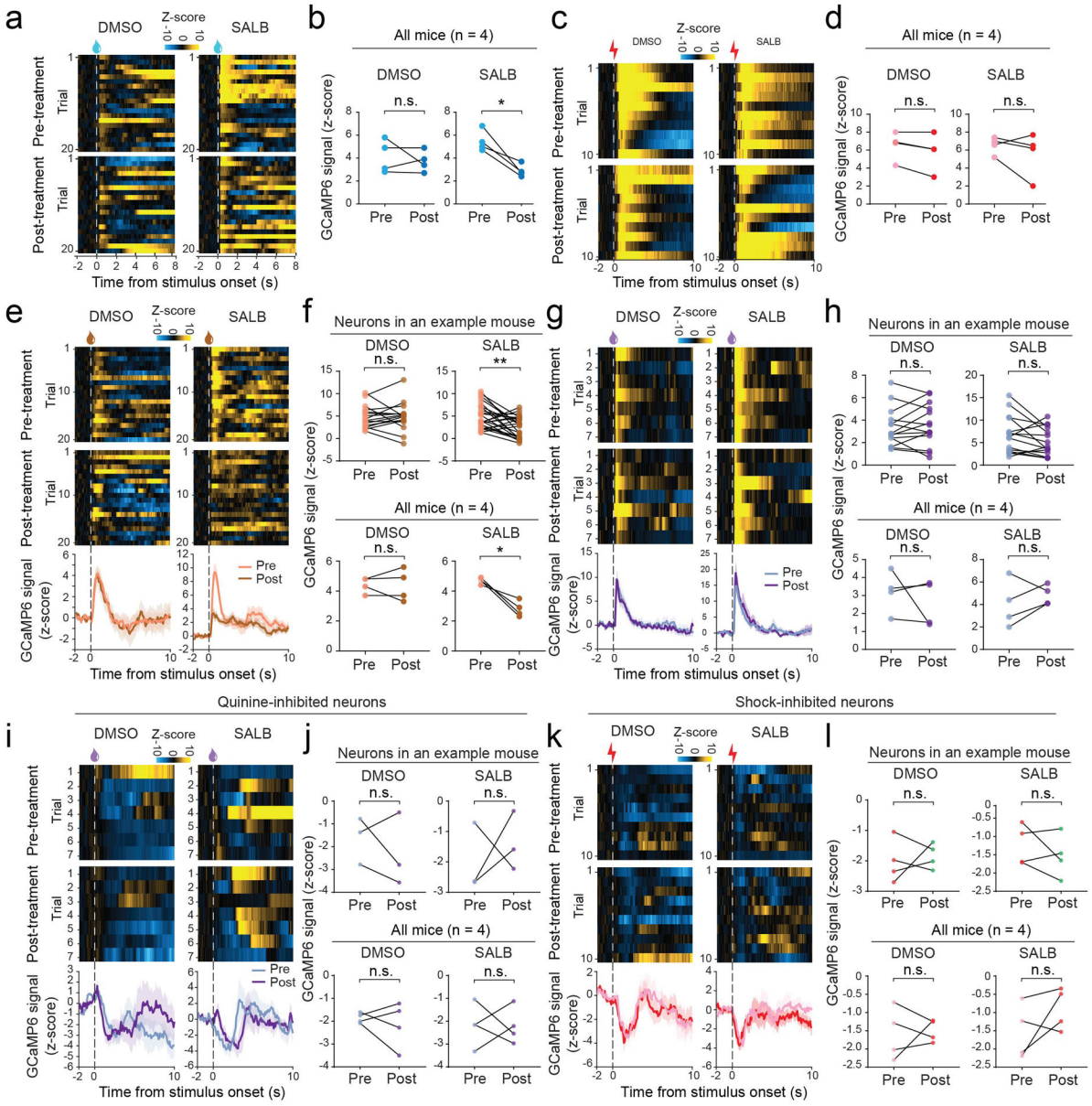

Extended Data Figure 9 |. DA neuron responses to appetitive stimuli are dependent on Sst^{+} CeA neurons.

a, Left: trial-by-trial activities of a water-excited neuron in a mouse receiving water, before (top) and after (bottom) the mouse was treated with DMSO. Right, trial-by-trial activities of another water-excited neuron in a mouse receiving water, before (top) and after (bottom) the mouse was treated with SALB. **b**, Quantification of the average water-evoked responses of all water-excited DA neurons in individual mice (n = 4 mice; DMSO, n.s., nonsignificant, P = 0.5807; SALB, *P = 0.0212; paired t-test). **c & d**, same as a & b, respectively, except that shock-excited neurons were analyzed, and mice received shock instead of water (quantification in d: n = 4 mice; DMSO, n.s., P = 0.0794; SALB, n.s., P = 0.3593; paired t-test). **e**, Left: trial-by-trial (top and middle) and average (bottom) activities of a sucrose-excited neuron in a mouse receiving sucrose, before and after the mouse was treated with

DMSO. Right: trial-by-trial (top and middle) and average (bottom) activities of another sucrose-excited neuron in a mouse receiving sucrose, before and after the mouse was treated with SALB. **f**, Top: Quantification of sucrose-induced responses in DA neurons in one example mouse. All DA neurons showing excitatory responses to sucrose were included (DMSO, n = 16 neurons, n.s., P = 0.8982; SALB, n = 25 neurons, **P = 0.0019; paired t-test). Bottom: quantification of the average sucrose-evoked responses of all sucrose-excited DA neurons in individual mice (n = 4 mice; DMSO, n.s., P = 0.9505; SALB, *P = 0.0132; paired t-test). **g & h,** same as e & f, respectively, except that quinine-excited neurons were analyzed, and mice received quinine instead of sucrose (quantification in h, top: DMSO, n = 14 neurons, n.s., P = 0.5657; SALB, n = 15 neurons, n.s., P = 0.0984; paired t-test; bottom: n = 4 mice; DMSO, n.s., P = 0.4903; SALB, n.s., P = 0.4020; paired t-test). **i & j**, same as g & h, respectively, except that quinine-inhibited neurons were analyzed (quantification in j, top: DMSO, n = 3 neurons, n.s., P = 0.7500; SALB, n = 3 neurons, n.s., P = 0.7500; Wilcoxon test; bottom: n = 4 mice; DMSO, n.s., P = 0.5906; SALB, n.s., P = 0.9527; paired t-test). **k & l**, same as i & j, respectively, except that shock-inhibited neurons were analyzed, and mice received shock instead of quinine (quantification in l, top: DMSO, n = 4 neurons, n.s., P = 0.6961; SALB, n = 4 neurons, n.s., P = 0.3916; paired t-test; bottom: n = 4 mice; DMSO, n.s., P = 0.8263; SALB, n.s., P = 0.2366; paired t-test).

Data are presented as mean ± s.e.m. Shaded areas represent s.e.m.

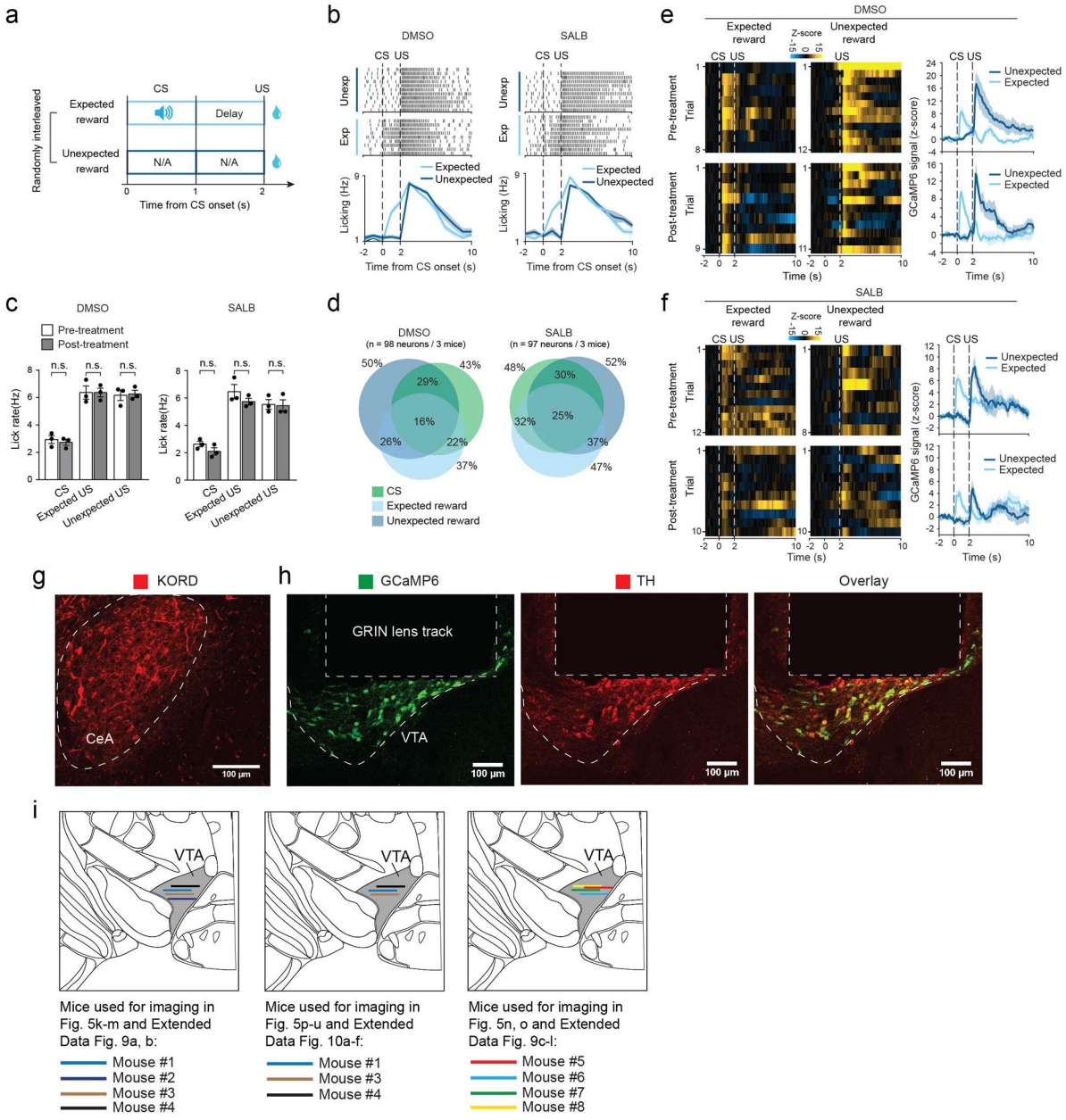

Extended Data Figure 10 l. Assessing the effects of Sst^{+} CeA neuron inhibition on DA neuron responses to expected and unexpected reward.

a, A schematic of the task. After mice were trained in the reward conditioning task where a sound predicted the delivery of water reward, they underwent an imaging session during which expected reward and unexpected reward were delivered in randomly interleaved trials. N/A, not applicable. **b**, Top and middle: raster plots of licking events for a mouse in unexpected-reward trials and expected-reward trials sorted according to trial types. The mouse was treated with DMSO (left) or SALB (right). Bottom: average licking rate of this mouse in different types of trials. Dashed lines indicate the onset of CS and US. **c**, Quantification of licking rate in a 2-s time window immediately after CS or US presentation in different conditions (n = 3 mice; DMSO: CS, P = 0.7133; expected US, P > 0.9999;

unexpected US, P = 0.7745; SALB: CS, P = 0.0572; expected US, P = 0.1317; unexpected US, P = 0.5799; n.s., nonsignificant; paired t-test). **d**, Percentage distributions of neurons excited by CS, expected reward, or unexpected reward, in mice treated with DMSO (left) or SALB (right). Fisher's exact test on the overlaps, DMSO: CS / expected reward, *P = 0.0121; CS / unexpected reward, **P = 0.0076; expected reward / unexpected reward, *P = 0.0119; SALB: CS / expected reward, ***P = 0.0005; CS / unexpected reward, P = 0.0680; expected reward / unexpected reward, ****P = 6.68e-07. **e**, Left and middle panels: heat-maps of trial-by-trial responses of a PE-encoding DA neuron in expected-reward trials (left) and unexpected-reward trials (middle), before (top) and after (bottom) the mouse was treated with DMSO. Right panel: average activity traces of this neuron in different trial types, before (top) and after (bottom) the mouse was treated with DMSO. **f**, same as **e**, except that SALB was used instead of DMSO to treat the mouse. **g-i,** Histology of the mice in which Sst^+ CeA neurons were chemogenetically inhibited and VTA DA neuron activity was imaged through a GRIN Lens. **g,** A confocal histological image of a coronal brain section from a representative mouse, showing the infection of Sst^+ CeA neurons with an AAV expressing KORD. **h,** Confocal histological images of a coronal brain section from a representative mouse, showing the infection of VTA DA neurons with an AAV expressing GCaMP6 (left), TH expression in DA neurons recognized with an antibody (middle). GCaMP6 expression was restricted in TH^+ neurons in the VTA (right). The track of GRIN lens implantation was indicated. **i**, Schematics showing the placement of GRIN lens implants in the VTA (n = 8 mice) used for the experiments. Note that some mice were used in more than one experiment, as indicated.

Data are presented as mean ± s.e.m. Shaded areas represent s.e.m.

Supplementary Material

Refer to Web version on PubMed Central for supplementary material.

Acknowledgements

We thank Radhashree Sharma for technical assistance and members of the Li laboratory for helpful discussions. This work was supported by grants from the National Institutes of Health (NIH) (R01MH101214, R01MH108924, R01NS104944, B.L.), Human Frontier Science Program (RGP0015/2016, B.L.), Wodecroft Foundation (B.L.), the Cold Spring Harbor Laboratory and Northwell Health Affiliation (B.L.), the Feil Family Neuroscience Endowment (B.L.), and OFIRG20nov-0030 from National Medical Research Council of Singapore (Y.F.).

Data availability

All data generated or analyzed during this study are included in this article (and its supplementary information files). Source data can be downloaded at https://figshare.com/articles/dataset/data_for_paper/21956900

Code availability

Source code can be downloaded at https://figshare.com/articles/software/code_for_paper/21956801

References

1. LeDoux JE The amygdala and emotion: A view through fear. In The Amygdala: A functional analysis (2nd edn) (Aggleton JP, ed.), pp. 289–310, Oxford University Press (2000).
2. Maren S. Building and burying fear memories in the brain. Neuroscientist 11, 89–99, doi:10.1177/1073858404269232 (2005). [PubMed: 15632281]
3. Fadok JP, Markovic M, Tovote P & Luthi A New perspectives on central amygdala function. Curr Opin Neurobiol 49, 141–147, doi:10.1016/j.conb.2018.02.009 (2018). [PubMed: 29522976]
4. Balleine BW & Killcross S Parallel incentive processing: an integrated view of amygdala function. Trends Neurosci 29, 272–279, doi:10.1016/j.tins.2006.03.002 (2006). [PubMed: 16545468]
5. Everitt BJ, Cardinal RN, Parkinson JA & Robbins TW Appetitive behavior: impact of amygdala-dependent mechanisms of emotional learning. Ann N Y Acad Sci 985, 233–250 (2003). [PubMed: 12724162]
6. Li B. Central amygdala cells for learning and expressing aversive emotional memories. Curr Opin Behav Sci 26, 40–45, doi:10.1016/j.cobeha.2018.09.012 (2019). [PubMed: 31011591]
7. Janak PH & Tye KM From circuits to behaviour in the amygdala. Nature 517, 284–292, doi:10.1038/nature14188 (2015). [PubMed: 25592533]
8. Herry C & Johansen JP Encoding of fear learning and memory in distributed neuronal circuits. Nat Neurosci 17, 1644–1654, doi:10.1038/nn.3869 (2014). [PubMed: 25413091]
9. Roesch MR, Esber GR, Li J, Daw ND & Schoenbaum G Surprise! Neural correlates of Pearce-Hall and Rescorla-Wagner coexist within the brain. Eur J Neurosci 35, 1190–1200, doi:10.1111/j.1460-9568.2011.07986.x (2012). [PubMed: 22487047]
10. Duvarci S & Pare D Amygdala microcircuits controlling learned fear. Neuron 82, 966–980, doi:10.1016/j.neuron.2014.04.042 (2014). [PubMed: 24908482]
11. Ciocchi S et al. Encoding of conditioned fear in central amygdala inhibitory circuits. Nature 468, 277–282, doi:10.1038/nature09559 (2010). [PubMed: 21068837]
12. Duvarci S, Popa D & Pare D Central amygdala activity during fear conditioning. J Neurosci 31, 289–294, doi:10.1523/JNEUROSCI.4985-10.2011 (2011). [PubMed: 21209214]
13. Iordanova MD, Deroche ML, Esber GR & Schoenbaum G Neural correlates of two different types of extinction learning in the amygdala central nucleus. Nat Commun 7, 12330, doi:10.1038/ncomms12330 (2016). [PubMed: 27531638]
14. Calu DJ, Roesch MR, Haney RZ, Holland PC & Schoenbaum G Neural correlates of variations in event processing during learning in central nucleus of amygdala. Neuron 68, 991–1001, doi:10.1016/j.neuron.2010.11.019 (2010). [PubMed: 21145010]
15. Shabel SJ & Janak PH Substantial similarity in amygdala neuronal activity during conditioned appetitive and aversive emotional arousal. Proc Natl Acad Sci U S A 106, 15031–15036, doi:10.1073/pnas.0905580106 (2009). [PubMed: 19706473]
16. Yu K. et al. The central amygdala controls learning in the lateral amygdala. Nat Neurosci 20, 1680–1685, doi:10.1038/s41593-017-0009-9 (2017). [PubMed: 29184202]
17. Steinberg EE et al. Amygdala-Midbrain Connections Modulate Appetitive and Aversive Learning. Neuron, doi:10.1016/j.neuron.2020.03.016 (2020).
18. Douglass AM et al. Central amygdala circuits modulate food consumption through a positive-valence mechanism. Nat Neurosci 20, 1384–1394, doi:10.1038/nn.4623 (2017). [PubMed: 28825719]
19. Yu K, Garcia da Silva P, Albeanu DF & Li B Central Amygdala Somatostatin Neurons Gate Passive and Active Defensive Behaviors. J Neurosci 36, 6488–6496, doi:10.1523/JNEUROSCI.4419-15.2016 (2016). [PubMed: 27307236]
20. Sadacca BF, Rothwax JT & Katz DB Sodium concentration coding gives way to evaluative coding in cortex and amygdala. J Neurosci 32, 9999–10011, doi:10.1523/JNEUROSCI.6059-11.2012 (2012). [PubMed: 22815514]
21. Cassell MD & Gray TS Morphology of peptide-immunoreactive neurons in the rat central nucleus of the amygdala. J Comp Neurol 281, 320–333, doi:10.1002/cne.902810212 (1989). [PubMed: 2468696]

22. Li H. et al. Experience-dependent modification of a central amygdala fear circuit. Nat Neurosci 16, 332–339, doi:10.1038/nn.3322 (2013). [PubMed: 23354330]
23. Haubensak W. et al. Genetic dissection of an amygdala microcircuit that gates conditioned fear. Nature 468, 270–276, doi:10.1038/nature09553 (2010). [PubMed: 21068836]
24. Penzo MA, Robert V & Li B Fear conditioning potentiates synaptic transmission onto long-range projection neurons in the lateral subdivision of central amygdala. J Neurosci 34, 2432–2437, doi:10.1523/JNEUROSCI.4166-13.2014 (2014). [PubMed: 24523533]
25. Penzo MA et al. The paraventricular thalamus controls a central amygdala fear circuit. Nature, doi:10.1038/nature13978 (2015).
26. Hartley ND et al. Dynamic remodeling of a basolateral-to-central amygdala glutamatergic circuit across fear states. Nat Neurosci 22, 2000–2012, doi:10.1038/s41593-019-0528-7 (2019). [PubMed: 31712775]
27. Kim J, Zhang X, Muralidhar S, LeBlanc SA & Tonegawa S Basolateral to Central Amygdala Neural Circuits for Appetitive Behaviors. Neuron 93, 1464–1479 e1465, doi:10.1016/j.neuron.2017.02.034 (2017). [PubMed: 28334609]
28. Zhou M. et al. A central amygdala to zona incerta projection is required for acquisition and remote recall of conditioned fear memory. Nat Neurosci 21, 1515–1519, doi:10.1038/s41593-018-0248-4 (2018). [PubMed: 30349111]
29. Shrestha P. et al. Amygdala inhibitory neurons as loci for translation in emotional memories. Nature 586, 407–411, doi:10.1038/s41586-020-2793-8 (2020). [PubMed: 33029009]
30. Fadok JP et al. A competitive inhibitory circuit for selection of active and passive fear responses. Nature 542, 96–100, doi:10.1038/nature21047 (2017). [PubMed: 28117439]
31. Venniro M. et al. Abstinence-dependent dissociable central amygdala microcircuits control drug craving. Proc Natl Acad Sci U S A 117, 8126–8134, doi:10.1073/pnas.2001615117 (2020). [PubMed: 32205443]
32. Chen TW et al. Ultrasensitive fluorescent proteins for imaging neuronal activity. Nature 499, 295–300, doi:10.1038/nature12354 (2013). [PubMed: 23868258]
33. Vankova M, Arluison M, Leviel V & Tramu G Afferent connections of the rat substantia nigra pars lateralis with special reference to peptide-containing neurons of the amygdalo-nigral pathway. J Chem Neuroanat 5, 39–50, doi:10.1016/0891-0618(92)90032-l (1992). [PubMed: 1376607]
34. Fudge JL & Haber SN The central nucleus of the amygdala projection to dopamine subpopulations in primates. Neuroscience 97, 479–494, doi:10.1016/s0306-4522(00)00092-0 (2000). [PubMed: 10828531]
35. Beier KT et al. Circuit Architecture of VTA Dopamine Neurons Revealed by Systematic Input-Output Mapping. Cell 162, 622–634, doi:10.1016/j.cell.2015.07.015 (2015). [PubMed: 26232228]
36. Lerner TN et al. Intact-Brain Analyses Reveal Distinct Information Carried by SNc Dopamine Subcircuits. Cell 162, 635–647, doi:10.1016/j.cell.2015.07.014 (2015). [PubMed: 26232229]
37. Watabe-Uchida M, Zhu L, Ogawa SK, Vamanrao A & Uchida N Whole-brain mapping of direct inputs to midbrain dopamine neurons. Neuron 74, 858–873, doi:10.1016/j.neuron.2012.03.017 (2012). [PubMed: 22681690]
38. Ogawa SK, Cohen JY, Hwang D, Uchida N & Watabe-Uchida M Organization of monosynaptic inputs to the serotonin and dopamine neuromodulatory systems. Cell Rep 8, 1105–1118, doi:10.1016/j.celrep.2014.06.042 (2014). [PubMed: 25108805]
39. Lau B, Monteiro T & Paton JJ The many worlds hypothesis of dopamine prediction error: implications of a parallel circuit architecture in the basal ganglia. Curr Opin Neurobiol 46, 241–247, doi:10.1016/j.conb.2017.08.015 (2017). [PubMed: 28985550]
40. Schultz W. Dopamine reward prediction error coding. Dialogues Clin Neurosci 18, 23–32 (2016). [PubMed: 27069377]
41. Vardy E. et al. A New DREADD Facilitates the Multiplexed Chemogenetic Interrogation of Behavior. Neuron 86, 936–946, doi:10.1016/j.neuron.2015.03.065 (2015). [PubMed: 25937170]
42. Deng H. et al. A genetically defined insula-brainstem circuit selectively controls motivational vigor. Cell 184, 6344–6360 e6318, doi:10.1016/j.cell.2021.11.019 (2021). [PubMed: 34890577]
43. Zhang X et al. Genetically identified amygdala-striatal circuits for valence-specific behaviors. Nat Neurosci 24, 1586–1600, doi:10.1038/s41593-021-00927-0 (2021). [PubMed: 34663958]

44. Zhang X & Li B Population coding of valence in the basolateral amygdala. Nat Commun 9, 5195, doi:10.1038/s41467-018-07679-9 (2018). [PubMed: 30518754]
45. Paton JJ, Belova MA, Morrison SE & Salzman CD The primate amygdala represents the positive and negative value of visual stimuli during learning. Nature 439, 865–870, doi:10.1038/nature04490 (2006). [PubMed: 16482160]
46. Murray JE et al. Basolateral and central amygdala differentially recruit and maintain dorsolateral striatum-dependent cocaine-seeking habits. Nat Commun 6, 10088, doi:10.1038/ncomms10088 (2015). [PubMed: 26657320]
47. Lingawi NW & Balleine BW Amygdala central nucleus interacts with dorsolateral striatum to regulate the acquisition of habits. J Neurosci 32, 1073–1081, doi:10.1523/JNEUROSCI.4806-11.2012 (2012). [PubMed: 22262905]
48. Wang Y. et al. Multimodal mapping of cell types and projections in the central nucleus of the amygdala. bioRxiv preprint *doi:* 10.1101/2022.10.19.512845 (2022).
49. Giovanniello J. et al. A central amygdala-globus pallidus circuit conveys unconditioned stimulus-related information and controls fear learning. J Neurosci, doi:10.1523/JNEUROSCI.2090-20.2020 (2020).
50. He M. et al. Cell-type-based analysis of microRNA profiles in the mouse brain. Neuron 73, 35–48, doi:10.1016/j.neuron.2011.11.010 (2012). [PubMed: 22243745]
51. Zeng WB et al. Anterograde monosynaptic transneuronal tracers derived from herpes simplex virus 1 strain H129. Mol Neurodegener 12, 38, doi:10.1186/s13024-017-0179-7 (2017). [PubMed: 28499404]
52. Li X. et al. Serotonin receptor 2c-expressing cells in the ventral CA1 control attention via innervation of the Edinger-Westphal nucleus. Nat Neurosci 21, 1239–1250, doi:10.1038/s41593-018-0207-0 (2018). [PubMed: 30104733]
53. Stephenson-Jones M. et al. A basal ganglia circuit for evaluating action outcomes. Nature 539, 289–293, doi:10.1038/nature19845 (2016). [PubMed: 27652894]
54. Xiong Q, Znamenskiy P & Zador AM Selective corticostriatal plasticity during acquisition of an auditory discrimination task. Nature 521, 348–351, doi:10.1038/nature14225 (2015). [PubMed: 25731173]
55. Znamenskiy P & Zador AM Corticostriatal neurons in auditory cortex drive decisions during auditory discrimination. Nature 497, 482–485, doi:10.1038/nature12077 (2013). [PubMed: 23636333]
56. Xiao X et al. A Genetically Defined Compartmentalized Striatal Direct Pathway for Negative Reinforcement. Cell 183, 211–227 e220, doi:10.1016/j.cell.2020.08.032 (2020). [PubMed: 32937106]
57. Keyes PC et al. Orchestrating Opiate-Associated Memories in Thalamic Circuits. Neuron 107, 1113–1123 e1114, doi:10.1016/j.neuron.2020.06.028 (2020). [PubMed: 32679036]
58. Pnevmatikakis EA & Giovannucci A NoRMCorre: An online algorithm for piecewise rigid motion correction of calcium imaging data. J Neurosci Methods 291, 83–94, doi:10.1016/j.jneumeth.2017.07.031 (2017). [PubMed: 28782629]
59. Pnevmatikakis EA et al. Simultaneous Denoising, Deconvolution, and Demixing of Calcium Imaging Data. Neuron 89, 285–299, doi:10.1016/j.neuron.2015.11.037 (2016). [PubMed: 26774160]
60. Zhou P. et al. Efficient and accurate extraction of in vivo calcium signals from microendoscopic video data. Elife 7, doi:10.7554/eLife.28728 (2018).
61. Gallistel CR, Fairhurst S & Balsam P The learning curve: implications of a quantitative analysis. Proc Natl Acad Sci U S A 101, 13124–13131, doi:10.1073/pnas.0404965101 (2004). [PubMed: 15331782]
62. Sheintuch L. et al. Tracking the Same Neurons across Multiple Days in Ca(2+) Imaging Data. Cell Rep 21, 1102–1115, doi:10.1016/j.celrep.2017.10.013 (2017). [PubMed: 29069591]
63. Rozeske RR et al. Prefrontal-Periaqueductal Gray-Projecting Neurons Mediate Context Fear Discrimination. Neuron 97, 898–910 e896, doi:10.1016/j.neuron.2017.12.044 (2018). [PubMed: 29398355]

64. Cunningham JP & Yu BM Dimensionality reduction for large-scale neural recordings. Nat Neurosci 17, 1500–1509, doi:10.1038/nn.3776 (2014). [PubMed: 25151264]

65. Allen WE et al. Thirst regulates motivated behavior through modulation of brainwide neural population dynamics. Science 364, 253, doi:10.1126/science.aav3932 (2019). [PubMed: 30948440]

66. Gao Z. et al. A cortico-cerebellar loop for motor planning. Nature 563, 113–116, doi:10.1038/s41586-018-0633-x (2018). [PubMed: 30333626]

67. Li N, Daie K, Svoboda K & Druckmann S Robust neuronal dynamics in premotor cortex during motor planning. Nature 532, 459–464, doi:10.1038/nature17643 (2016). [PubMed: 27074502]

68. Kim CK et al. Simultaneous fast measurement of circuit dynamics at multiple sites across the mammalian brain. Nature methods 13, 325–328, doi:10.1038/nmeth.3770 (2016). [PubMed: 26878381]

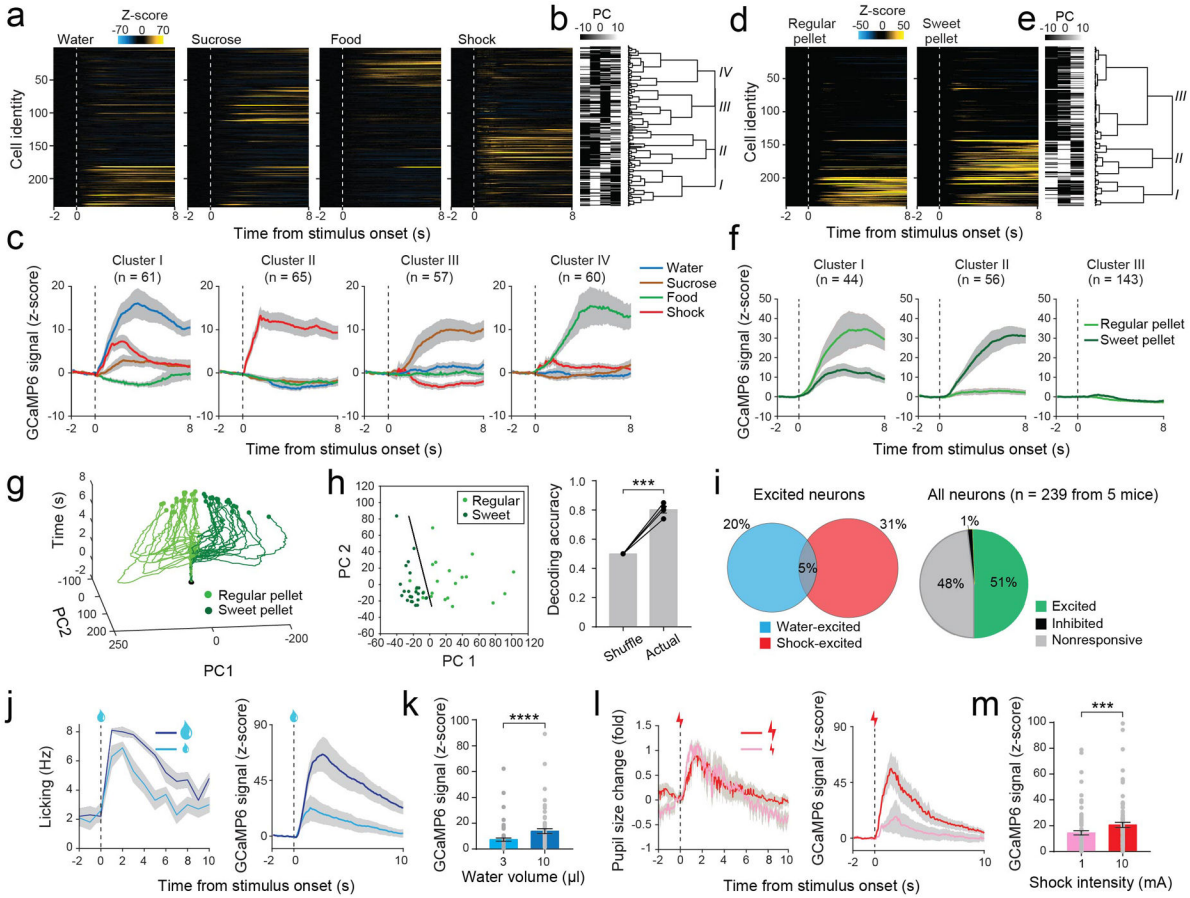

Figure 1 |. The encoding properties of Sst^{+} CeA neurons.

a, Heat-maps of the responses to different stimuli. Each row represents the activities of one neuron. **b**, The first four principle components (PC) (explaining 83% of the variance) and hierarchical clustering dendrogram. **c**, Average responses of each cluster to different stimuli (n = 243 neurons/4 mice). **d**, Heat-maps of the responses to regular pellet and sweet pellet. Each row represents the activities of one neuron. **e**, The first three PCs (explaining 96% of the variance) and hierarchical clustering dendrogram. **f**, Average responses of each cluster to different pellets (n = 243 neurons/4 mice). **g**, The trajectories of trial-by-trial population neuronal responses to regular pellet and sweet pellet. Data were from a representative mouse. Black dots indicate stimulus onset. **h**, Left, an example SVM decoding using neuronal population activities in response to regular pellet and sweet pellet. Right, performance of decoding using actual neuronal responses to regular pellet and sweet pellet, or using neuronal responses shuffled across trial types (n = 4 mice, ***P = 0.0010, paired t-test). **i**, Left: percentage distribution of neurons excited by water or shock (Fisher's exact test on the overlap, P = 0.3840). Right: percentage distributions of neurons excited or inhibited by water or shock, and nonresponsive neurons. **j**, Left: licking rate of a mouse in response to different volumes of water. Right: responses of a water-excited neuron. **k**, Average peak responses of water-excited neurons to different volumes of water (****P = 7.34e-07, Wilcoxon test). **l**, Left: pupil size change of a mouse in response to tail shock.

Right: the responses of a shock-excited neuron. **m**, Average peak responses of shock-excited neurons to different intensities of tail shock (***P = 0.0001, Wilcoxon test).
Data are presented as mean ± s.e.m. Shaded areas represent s.e.m.

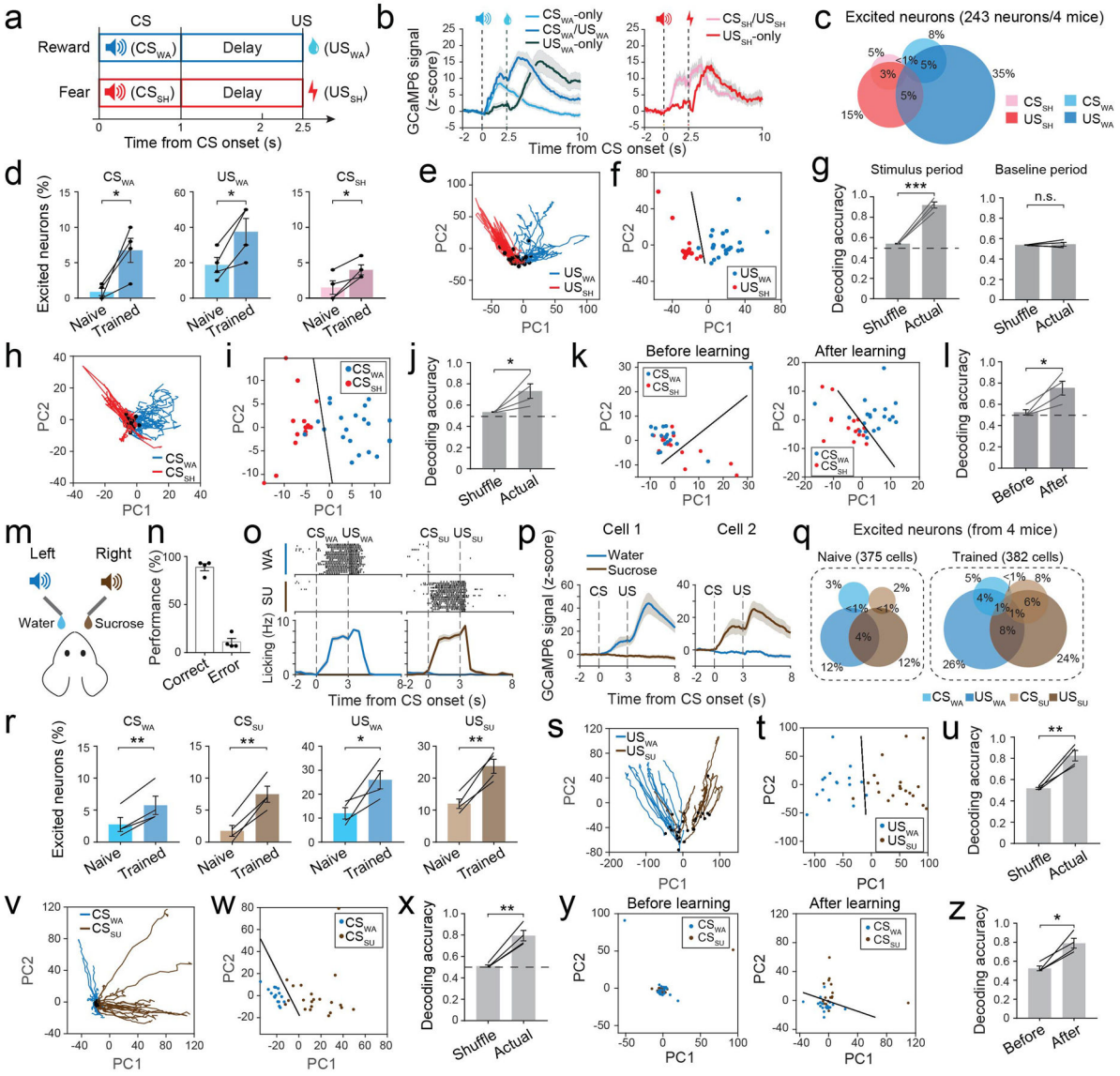

Figure 2 | Learning-dependent and stimulus-specific encoding.

a, A task schematic. **b**, Activity traces after reward (left) or fear (right) conditioning. **c**, Percentage distributions after training (Fisher's exact test: CS_{WA}/CS_{SH}, P > 0.9999; US_{WA}/US_{SH}, P > 0.9999; CS_{WA}/US_{WA}, **P = 0.004; CS_{SH}/US_{SH}, ****P = 1.2e-06). **d**, Quantification of excited neurons (n = 4 mice; CS_{WA}, *P = 0.0371; US_{WA}, *P = 0.0358; CS_{SH}, *P = 0.0305; paired t-test). **e**, Population response trajectories after training. Black dots indicate US onset. **f**, An example SVM decoding. **g**, Decoding performance using US responses (left, n = 4 mice, ***P = 0.0008) or baseline activities (right, n.s., nonsignificant, P = 0.6971; paired t-test). **h, i, j**, same as e, f, g (left), respectively, except that CS responses were used (*P = 0.0305). **k**, **l**, Example SVM decoding (k) and decoding performance (l) across learning (n = 98 tracked neurons/4 mice, *P = 0.0359, paired t-test). **m**, A task schematic. **n**, Mouse performance (n = 4). **o**, Lick raster (top, middle) and average licking rate (bottom) of a mouse. **p**, Neuronal activity traces. **q**, Percentage distributions (Fisher's

exact test, naïve: CS_{WA}/CS_{SU}, P > 0.9999; US_{WA}/US_{SU}, ****P = 4.05e-05; CS_{WA}/US_{WA}, P = 0.6711; CS_{SU}/US_{SU}, P = 0.3630; trained: CS_{WA}/CS_{SU}, P = 0.7007; US_{WA}/US_{SU}, P = 0.0763; CS_{WA}/US_{WA}, ****P = 1.02e-06; CS_{SU}/US_{SU}, ****P = 8.93e-10). **r**, Quantification of neurons (n = 4 mice; CS_{WA}, **P = 0.0052; US_{WA}, *P = 0.0431; CS_{SU}, **P = 0.0046; US_{SU}, **P = 0.0057; paired t-test). **s**, Responses trajectories after training. Black dots indicate US onset. **t**, An example SVM decoding. **u**, Decoding performance (n = 4 mice, **P = 0.0080, paired t-test). **v, w, x**, Same as s, t, u, respectively, except that CS responses were used (**P = 0.0054). **y**, Example SVM decoding. **z**, Learning improved decoding accuracy (n = 4 mice, *P = 0.0174, paired t-test).

Data are presented as mean ± s.e.m. Shaded areas represent s.e.m.

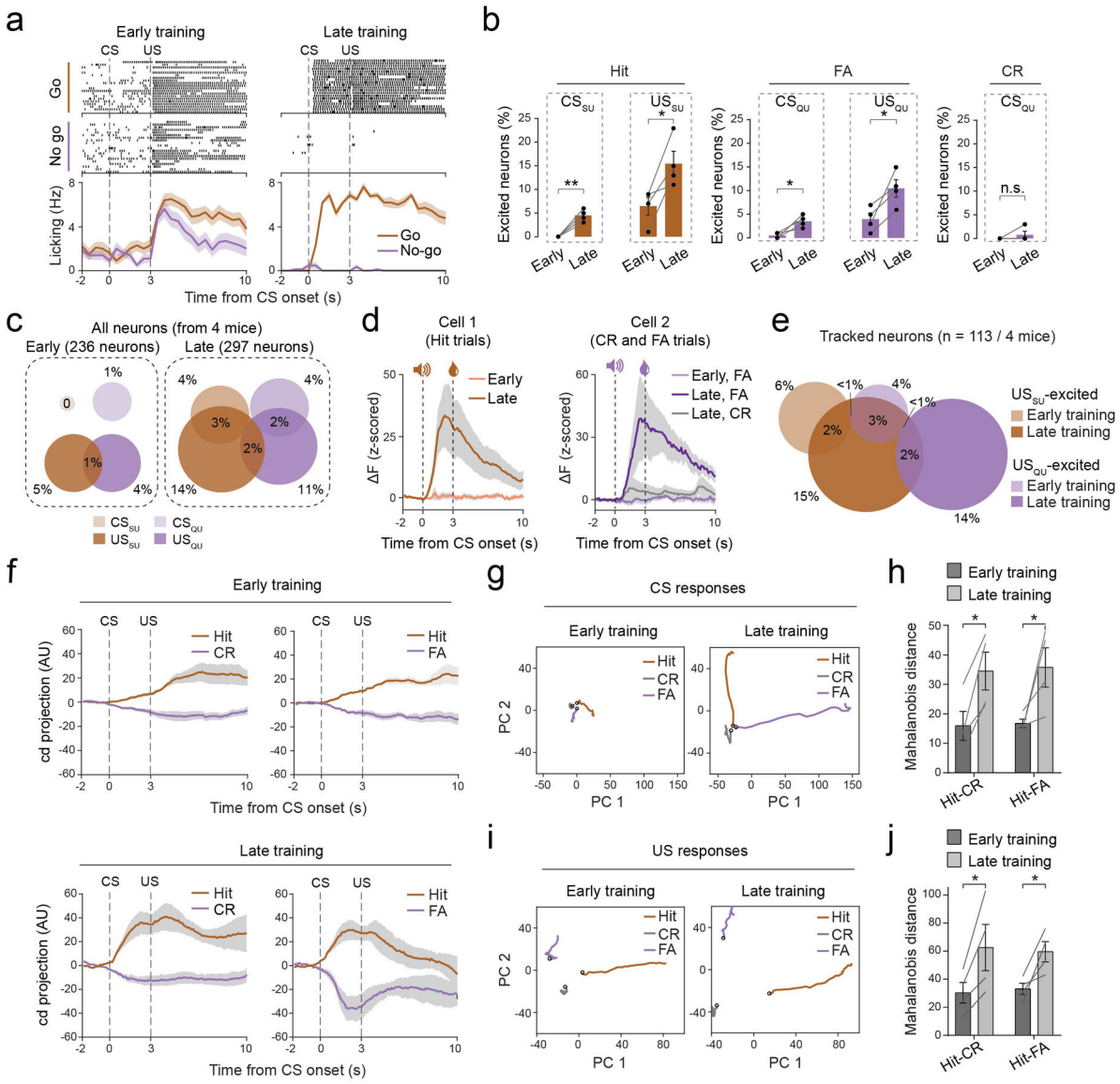

Figure 3 | Learning induces and transforms US responses.

a, Top: licking events of a mouse at the early (left) and late (right) training stages in the go/no-go task. Bottom: average licking rate. **b**, Quantification of excited neurons across training (n = 4 mice; hit, CS_{SU}, **P = 0.0061, US_{SU}, *P = 0.0424; false alarm (FA), CS_{QU}, *P = 0.0349, US_{QU}, *P = 0.0390; correct rejection (CR), CS_{QU}, n.s., nonsignificant, P = 0.39; paired t-test). **c**, Percentage distributions of excited neurons at early (left) and late (right) training stages (Fisher's exact test, early stage: CS_{SU}/CS_{QU}, P > 0.9999; US_{SU}/US_{QU}, P = 0.1533; CS_{SU}/US_{SU}, P > 0.9999; CS_{QU}/US_{QU}, P > 0.9999; late stage: CS_{SU}/CS_{QU}, P > 0.9999; US_{SU}/US_{QU}, P = 0.4242; CS_{SU}/US_{SU}, ****P = 1.61e-06; CS_{QU}/US_{QU}, ***P = 0.0007). **d**, Activity traces of two tracked neurons across training. **e**, Percentage distributions of the tracked neurons across training (Fisher's exact test: early US_{SU} /late US_{SU}, P = 0.2833; early US_{QU} /late US_{QU}, P > 0.9999; early US_{SU} /early US_{QU}, P = 0.2780; late US_{SU} /late US_{QU}, P > 0.9999; early US_{SU} /late US_{QU}, P = 0.5906; early US_{QU} /late

US_{SU}, *P = 0.0238). **f**, Neuronal activities projected onto coding direction (***cd***), at early (top) and late (bottom) training stages. AU, arbitrary unit. **g**, Population CS responses of neurons from one mouse before (left) and after (right) learning. PC, principal components. **h**, Quantification of the Mahalanobis distance between CS responses (n = 4 mice; F(1,6) = 19.47, P = 0.0045; hit-CR, *P = 0.0430, hit-FA, *P = 0.0393; two-way ANOVA followed by Sidak's test). **i**, **j**, Same as g, h, respectively, except that US responses were analyzed (F(1,6) = 22.94, P = 0.0030; hit-CR, *P = 0.0198, hit-FA, *P = 0.0447).

Data are presented as mean ± s.e.m. Shaded areas represent s.e.m.

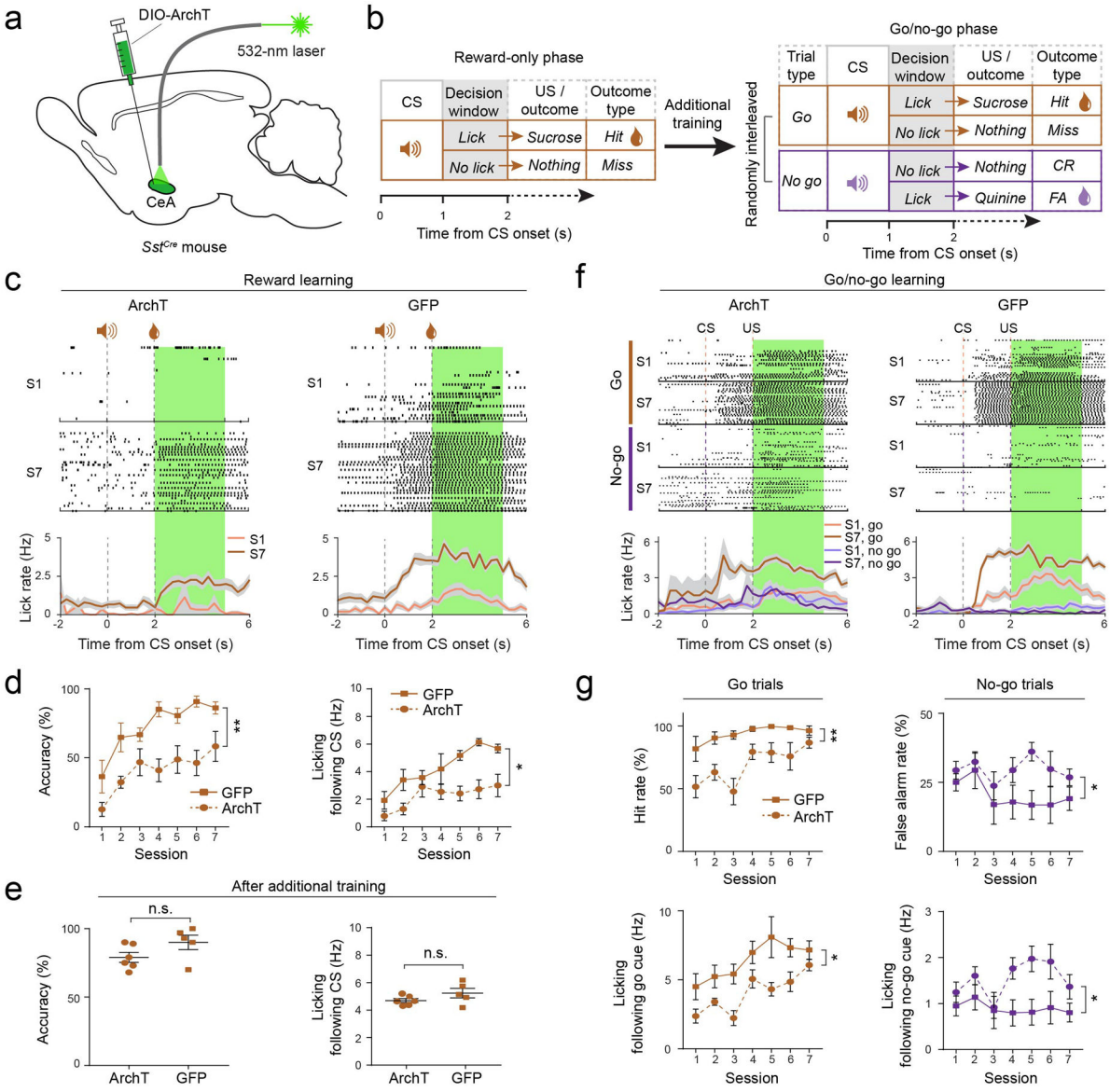

Figure 4 |. The US response of Sst$^+$ CeA neurons facilitates reward and aversive learning.

a, b, Schematics of the approach (a) and task design (b). **c**, Top: lick raster of an ArchT mouse (left) and GFP mouse (right) in session 1 (S1) and 7 (S7) during reward-only training. Bottom: average licking rates of the same mice. Green shaded area indicates the time window when laser was turned on. **d**, Left, performance across reward-only training sessions (ArchT group, n = 6 mice, GFP group, n = 5 mice; F(1,9) = 18.91, **P = 0.0019; two-way ANOVA followed by Sidak's test). Right, licking rates following CS onset across training sessions (F(1,9) = 10.25, *P = 0.0108; two-way ANOVA followed by Sidak's test). **e**, The same mice in d were subjected to additional training in the absence of laser, and reached similar levels of performance (left) and anticipatory licking (right) (n.s., nonsignificant, p > 0.05, t-test). **f**, Top: lick raster of an ArchT mouse (left) and GFP mouse (right) during go/no-go training. Bottom: average licking rates of the same mice. Green shaded area indicates the time window when laser was turned on. **g**, Top left, hit rate across training

sessions (ArchT group, n = 6 mice, GFP group, n = 5 mice; F(1,9) = 15.78, **P = 0.003; two-way ANOVA followed by Sidak's test). Bottom left, licking rate following CS onset in go trials across training sessions (F(1,9) =10.25, *P = 0.01; two-way ANOVA followed by Sidak's test). Top right, false alarm rate across training sessions (F(1,9) = 6.736, *P = 0.02; two-way ANOVA followed by Sidak's test). Bottom right, licking rate following CS onset in no-go trials across training sessions (F(1,9) =7.57, *P = 0.02; two-way ANOVA followed by Sidak's test).

Data are presented as mean ± s.e.m. Shaded areas represent s.e.m.

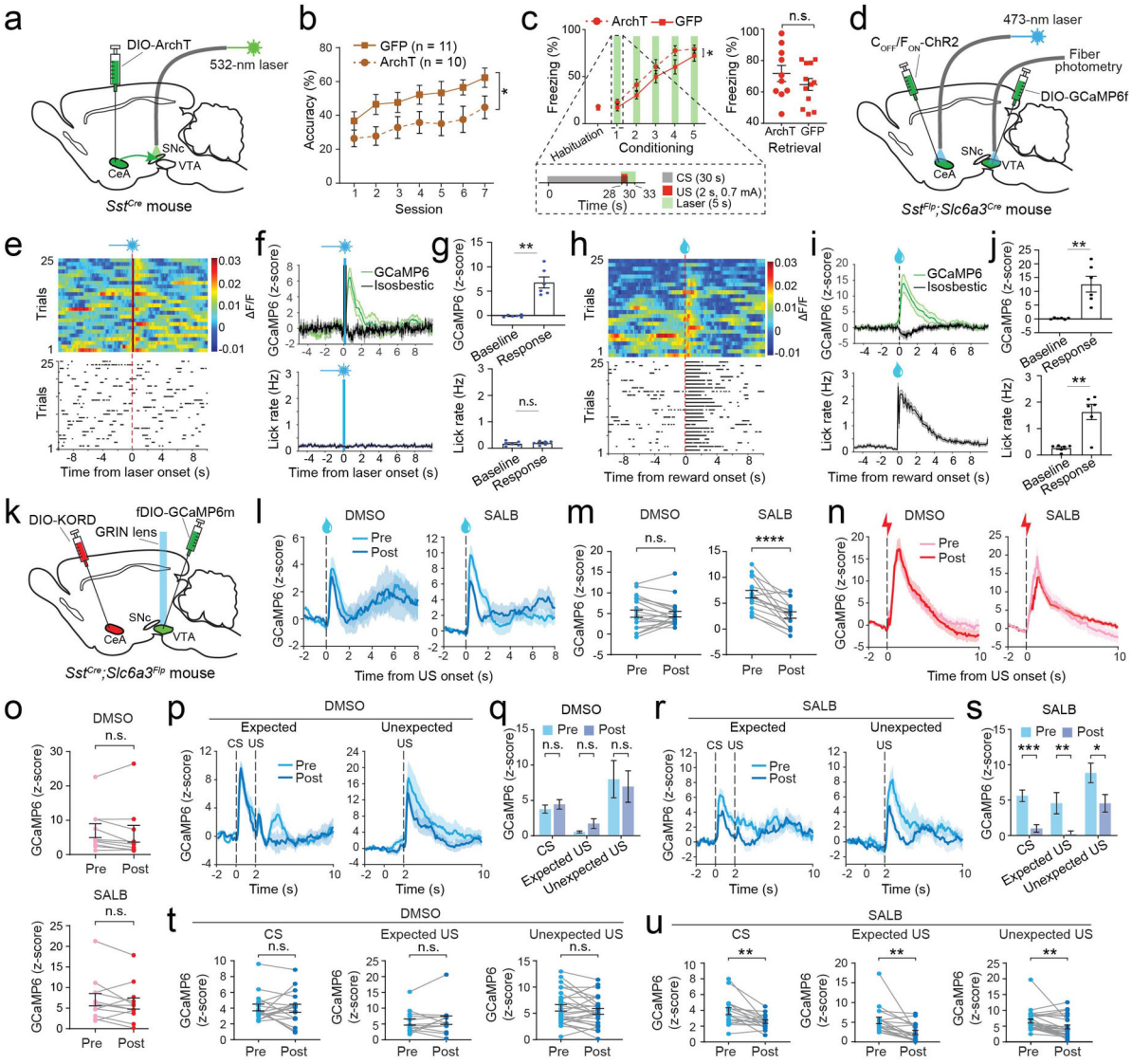

Figure 5 l. Sst$^{CeA\rightarrow DA}$ regulates reward learning and DA neurons.

a, A schematic of the approach. **b**, Performance across reward-only training (ArchT, n = 10 mice; GFP, n = 11 mice; F(1,19) = 5.368, *P = 0.0318; two-way ANOVA). **c**, Freezing during fear conditioning (F(1,19) = 6.874, *P = 0.0168, two-way ANOVA) and retrieval (n.s., nonsignificant, P = 0.4994, Mann-Whitney test). **d**, A schematic of the approach. **e**, Trial-by-trial DA-neuron activity (top) and licking (bottom) of one mouse. **f**, Average DA-neuron activity (top) and licking rate (bottom). **g**, Quantification of neural activities (top) and licking (bottom) (n = 6 mice, **P = 0.0018, n.s., P = 0.2212; paired t-test). **h, i, j**, same as e, f, g, respectively, except that water was used (n = 6 mice; neural activities, **P = 0.0076; licking, **P = 0.0027). **k**, A schematic of the approach. **l**, Water-evoked responses of a neuron. **m**, Quantification of water-induced responses in one mouse (DMSO, n = 20 neurons, n.s., P = 0.8430; SALB, n = 17 neurons, **** P = 3.73e-05; paired t-test). **n, o**, same as l, m, respectively, except that shock-evoked responses were analyzed (DMSO, n = 10 neurons, n.s., P = 0.2130; SALB, n = 12 neurons, n.s., P = 0.2381). **p**, Responses of a

PE-encoding neuron. **q**, Quantification of PE-encoding neuron responses (n = 4 neurons/3 mice; CS, n.s., P = 0.3361; expected US, n.s., P = 0.2435; unexpected US, n.s., P = 0.4477; paired t-test). **r**, **s**, same as p, q, respectively, except that SALB was used (n = 7 neurons/3 mice; CS, ***P = 0.0005; expected US, **P = 0.0061; unexpected US, *P = 0.0200). **t**, **u**, Quantification of the responses in one mouse under DMSO (CS, n = 17 neurons, n.s., P = 0.8380; expected US, n = 13 neurons, n.s., P = 0.4903; unexpected US, n = 26 neurons, n.s., P = 0.1318) or SALB (CS, n = 17 neurons, **P = 0.0033; expected US, n = 18 neurons, **P = 0.0015; unexpected US, n = 27 neurons, **P = 0.0040; paired t-test).
Data are presented as mean ± s.e.m. Shaded areas represent s.e.m.